



UNIVERSITY OF LEEDS

This is a repository copy of *Decaying Lava Extrusion Rate at El Reventador Volcano, Ecuador, Measured Using High-Resolution Satellite Radar*.

White Rose Research Online URL for this paper:  
<http://eprints.whiterose.ac.uk/124812/>

Version: Accepted Version

---

**Article:**

Arnold, DWD, Biggs, J, Anderson, K et al. (5 more authors) (2017) Decaying Lava Extrusion Rate at El Reventador Volcano, Ecuador, Measured Using High-Resolution Satellite Radar. *Journal of Geophysical Research. Solid Earth*, 122 (12). pp. 9966-9988. ISSN 2169-9356

<https://doi.org/10.1002/2017JB014580>

---

© 2017. American Geophysical Union. All Rights Reserved. This is an author produced version of a paper published in *Journal of Geophysical Research. Solid Earth*. Uploaded in accordance with the publisher's self-archiving policy.

**Reuse**

Items deposited in White Rose Research Online are protected by copyright, with all rights reserved unless indicated otherwise. They may be downloaded and/or printed for private study, or other acts as permitted by national copyright laws. The publisher or other rights holders may allow further reproduction and re-use of the full text version. This is indicated by the licence information on the White Rose Research Online record for the item.

**Takedown**

If you consider content in White Rose Research Online to be in breach of UK law, please notify us by emailing [eprints@whiterose.ac.uk](mailto:eprints@whiterose.ac.uk) including the URL of the record and the reason for the withdrawal request.



[eprints@whiterose.ac.uk](mailto:eprints@whiterose.ac.uk)  
<https://eprints.whiterose.ac.uk/>

# Decaying lava extrusion rate at El Reventador Volcano, Ecuador measured using high-resolution satellite radar

D.W.D. Arnold<sup>1</sup>, J. Biggs<sup>1</sup>, K. Anderson<sup>2</sup>, S. Vallejo Vargas<sup>3,4</sup>, G. Wadge<sup>5</sup>, S.K. Ebmeier<sup>1,6</sup>,  
M.F. Naranjo<sup>3</sup>, P. Mothes<sup>3</sup>

<sup>1</sup>COMET, School of Earth Sciences, University of Bristol, Bristol, UK

<sup>2</sup>USGS, California Volcano Observatory, Menlo Park, California, USA

<sup>3</sup>Instituto Geofísico, Escuela Politécnica Nacional, Quito, Ecuador

<sup>4</sup>LMV, Université Clermont Auvergne, Clermont-Ferrand, France

<sup>5</sup>COMET, Department of Meteorology, University of Reading, Reading, UK

<sup>6</sup>COMET, School of Earth and Environment, University of Leeds, Leeds, UK

## Key Points:

- High resolution satellite radar measures extruded lava volume at the andesitic El Reventador stratovolcano at 11 day to 10 month intervals
- The time-averaged lava extrusion rate decays gradually over the 4 year observation period
- We fit the extrusion rate with a model of a depressurising reservoir, with constant magma influx from below at rates less than  $0.35 \text{ m}^3\text{s}^{-1}$

---

Corresponding author: David Arnold, david.arnold@bristol.ac.uk

## 18 Abstract

19 Lava extrusion at erupting volcanoes causes rapid changes in topography and morphol-  
 20 ogy on the order of tens or even hundreds of metres. Satellite radar provides a method  
 21 for measuring changes in topographic height over a given time period to an accuracy of  
 22 metres, either by measuring the width of radar shadow cast by steep sided features, or  
 23 by measuring the difference in radar phase between two sensors separated in space. We  
 24 measure height changes, and hence estimate extruded lava volume flux, at El Reventador,  
 25 Ecuador between 2011 and 2016, using data from the Radarsat-2 and TanDEM-X satel-  
 26 lite missions. We find 39 new lava flows were extruded between 9 February 2012 and 24  
 27 August 2016, with a cumulative volume of 44.8M m<sup>3</sup> dense rock equivalent and a grad-  
 28 ually decreasing eruption rate. The average dense rock rate of lava extrusion during this  
 29 time is  $0.31 \pm 0.02 \text{ m}^3\text{s}^{-1}$ , which is similar to the long term average from 1972 to 2016.  
 30 Apart from a volumetrically small dyke opening event between 9 March and 10 June  
 31 2012, lava extrusion at El Reventador is not accompanied by any significant magmatic  
 32 ground deformation. We use a simple physics-based model to estimate that the volume of  
 33 the magma reservoir under El Reventador is greater than 3 km<sup>3</sup>. Our lava extrusion data  
 34 can be equally well fit by models representing a closed reservoir depressurising during  
 35 the eruption with no magma recharge, or an open reservoir with a time-constant magma  
 36 recharge rate of up to  $0.35 \pm 0.01 \text{ m}^3\text{s}^{-1}$ .

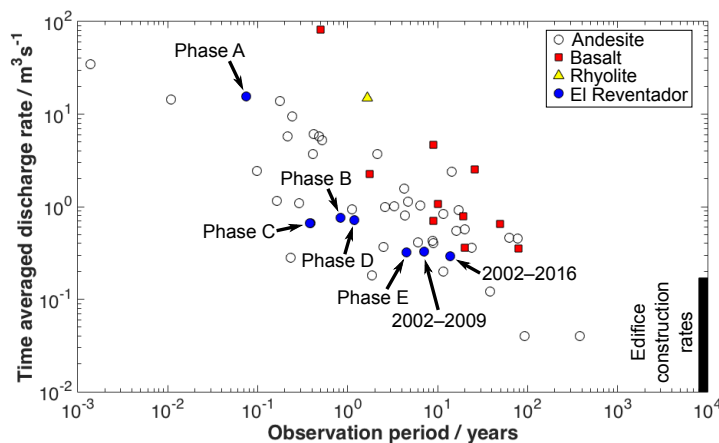
## 37 1 Introduction

38 The rate of lava extrusion at erupting volcanoes is a key parameter for tracking  
 39 changes in magma flux, eruptive behaviour, and associated hazards, through time [e.g.  
 40 *Walker et al., 1973; Fink and Griffiths, 1998; Cashman and Sparks, 2013*]. The lava extru-  
 41 sion rate exerts a critical influence on the length and extent of lava flows, and can provide  
 42 insight into the dimensions and depth of the volcanic reservoir and conduit [*Walker et al.,*  
 43 *1973; Harris et al., 2007; Poland, 2014*]. At long-lived eruptions, variations in extrusion  
 44 rate may give an indication of changes to the volcanic plumbing system or magma supply  
 45 rate, and potentially an estimation of when declining eruptions may finish [*Harris et al.,*  
 46 *2003; Wadge et al., 2006a; Gudmundsson et al., 2016*].

47 Variations in lava extrusion rate have been observed on timescales varying from  
 48 minutes through to decades (Supplementary Table S1). On timescales of minutes to days,  
 49 these fluctuations are generally due to shallow processes involving magma supply to the

50 surface through a conduit with physical properties that can vary with time [Voight *et al.*,  
 51 1998; Nakada *et al.*, 1999; Johnson *et al.*, 2008; Anderson *et al.*, 2010; Hautmann *et al.*,  
 52 2013; Walter *et al.*, 2013]. Over longer timescales, variations are thought to be caused  
 53 by processes involving magma supply from the lower crust or mantle [e.g. Dvorak and  
 54 Dzurisin, 1993; Harris *et al.*, 2003; Poland *et al.*, 2012; Poland, 2014].

55 Many volcanoes erupt at rates that are constant when averaged over years or decades  
 56 ( $0.1\text{--}2\text{ m}^3\text{s}^{-1}$ ), regardless of magma composition or tectonic setting, presumably because  
 57 this is the constant long term supply rate of melt buoyantly rising through the crust [Wadge,  
 58 1982; Sheldrake *et al.*, 2016]. Figure 1 and Supplementary Table S1 show a compila-  
 59 tion of previously measured time-averaged extrusion rates over a range of measurement  
 60 timescales. Longer measurement periods tend to give lower average extrusion rates, as  
 61 pulses of high instantaneous lava flux are averaged out by intervening periods of much  
 62 lower flux or quiescence intervals of no lava extrusion. We expect the trend of decreasing  
 63 time-averaged discharge rate with observation time to plateau at increasingly longer ob-  
 64 servation times, as the observed extruded lava converges on the long term magma supply  
 65 rate, estimated to be  $0.01\text{--}0.1\text{ m}^3\text{s}^{-1}$  for most volcanoes from volcanic edifice construction  
 66 rates measured over timescales of  $10^4$  years or longer [e.g. Wadge, 1982; Thouret, 1999].



67 **Figure 1.** Time-averaged eruption rate from historical eruptions, plotted against the duration of observation  
 68 period. Recent eruptive phases of El Reventador are labelled. Sources for the data are given in Supplementary  
 69 Table S1. The black bar shows the range of long-term volcanic edifice construction rates, which occur over  
 70 timescales of  $10^4$  to  $10^6$  years [Thouret, 1999].

71 Magma or volatiles entering or leaving a subsurface magma reservoir will cause a  
72 pressure change within the reservoir, which can lead to deformation of the ground surface  
73 [e.g. *Dzurisin, 2003; Pinel et al., 2014*]. In an elastic crust, a volcanic eruption draining a  
74 single magma reservoir, with flow through the conduit proportional to reservoir pressure,  
75 will have an exponentially decaying extrusion rate and a deflation signal that also decays  
76 exponentially through time [e.g. *Dvorak and Okamura, 1987; Mastin et al., 2009; Ander-*  
77 *son and Segall, 2013; Hreinsdóttir et al., 2014*].

78 Many volcanic eruptions are relatively short duration (weeks-months), and can typ-  
79 ically be modelled by the depletion of one or more finite (closed) magma reservoirs be-  
80 neath the volcano [e.g. *Rymer and Williams-Jones, 2000; Dzurisin, 2003; Chaussard et al.,*  
81 *2013*]. The spatial and temporal pattern and magnitude of volcanic deformation can be  
82 modelled using simple analytical elastic half-space models [e.g. *Mogi, 1958; Okada, 1985*]  
83 or more complex numerical methods [e.g. *Dieterich and Decker, 1975; Gottsmann et al.,*  
84 *2006; Hickey and Gottsmann, 2014*] to constrain the source reservoir location and geome-  
85 try. Kinematic deformation source models can be incorporated into physics-based models  
86 that include the physics of magmatic processes and and can be used to naturally model  
87 the temporal evolution of deformation signals [e.g. *Huppert and Woods, 2002; Anderson*  
88 *and Segall, 2013; Segall, 2013; Anderson and Poland, 2016*]. Models that do not include  
89 magma physics cannot naturally replicate this temporal evolution of the system [*Segall,*  
90 *2013*].

91 Alternatively, volcanoes can behave as open systems, with persistent or frequent mi-  
92 nor eruptions and degassing which can persist for decades, with little to no ground de-  
93 formation [e.g. *Pritchard and Simons, 2002; Moran et al., 2006; Fournier et al., 2010;*  
94 *Pinel et al., 2011; Chaussard et al., 2013; Ebmeier et al., 2013a; Biggs et al., 2014*]. The  
95 lack of observed ground deformation at these systems implies a lack of pressure change  
96 in the shallow system, possibly because of the high compressibility of volatile rich mag-  
97 mas, deep storage of melts that rise rapidly to the surface without intrusion in the upper  
98 crust, or temporal aliasing of deformation observations, which do not capture short-term  
99 transient deformation episodes [*Chaussard et al., 2013; Ebmeier et al., 2013a; Biggs et al.,*  
100 *2014; McCormick-Kilbride et al., 2016*].

101 Shorter-term transient deformation processes, associated with the magma conduit  
102 and lava dome, have been observed at long-lived andesitic dome forming eruptions, such

103 as Montserrat, Colima and Santiaguio [Voight *et al.*, 1998; Johnson *et al.*, 2008; Sanderson  
104 *et al.*, 2010; Walter *et al.*, 2013; Salzer *et al.*, 2014]. These transient processes occur on  
105 timescales of minutes to hours and are usually shallow and therefore only deform the area  
106 proximal to the active lava dome, making them difficult to detect with infrequent satel-  
107 lite observations, or distal ground based monitoring instruments [Dzurisin, 2003; Segall,  
108 2005].

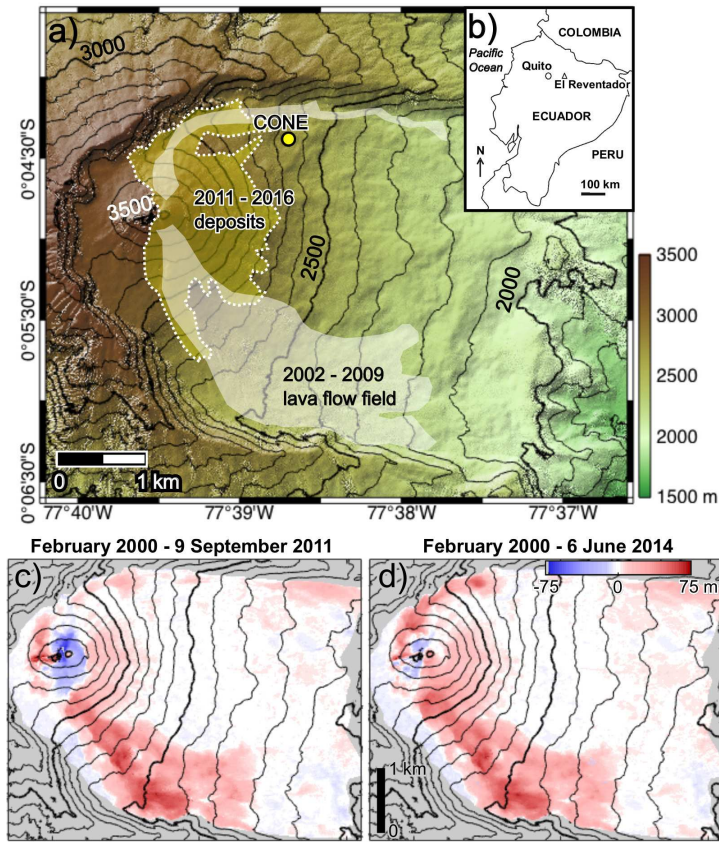
109 Long-lived volcanic eruptions provide an ideal target for studying the evolution of  
110 open systems with time, the transitions between extrusive and explosive behaviour and the  
111 underlying causes driving any changes, such as variations in magma supply rate, magma  
112 composition, and surface morphology [Watts *et al.*, 2002; Cashman and Sparks, 2013;  
113 Segall, 2013]. In this study, we use high-resolution radar satellite imagery to investigate  
114 the time-averaged lava extrusion rate, ground deformation and magma supply rate at the  
115 long-lived eruption of El Reventador, Ecuador

## 127 **2 El Reventador background**

128 El Reventador is a stratovolcano of basaltic-andesite to andesitic composition, sit-  
129 uated in the Cordillera Real approximately 90 km east of Quito (Fig. 2b), and is one of  
130 the most active volcanoes in Ecuador, with more than 20 historical eruptive episodes since  
131 1600 [Simkin *et al.*, 1981]. Following minor eruptive activity in the 1970s, the most re-  
132 cent eruptive period at El Reventador began with a subplinian explosion on November 3  
133 2002, which has been followed by semi-continuous eruptive behaviour that is ongoing at  
134 the time of writing (Smithsonian GVP/IG-EPN activity reports).

135 The initial eruption began with little precursory surface or seismic activity, and  
136 generated an ash plume that rose to 17 km and pyroclastic density currents which trav-  
137 elled up to 9 km from the vent [Hall *et al.*, 2004]. Subsequent eruptive behaviour has  
138 been dominated by the extrusion of blocky basaltic andesite and andesitic lava flows, lava  
139 dome growth and minor Strombolian explosions [Hall *et al.*, 2004; Ridolfi *et al.*, 2008;  
140 Samaniego *et al.*, 2008; Naranjo *et al.*, 2016]. Petrological analysis of products from the  
141 2002 eruption suggests that there was a single pre-eruptive reservoir with a top at  $8 \pm 2$   
142 km and a base at  $11 \pm 2$  km [Ridolfi *et al.*, 2008; Samaniego *et al.*, 2008].

143 Naranjo *et al.* [2016] mapped and measured lava flows extruded in 4 phases (A–D)  
144 of activity between 2002 and 2009 at El Reventador, which each lasted 1–20 months and



116 **Figure 2.** a) Hillshaded Digital Elevation Model (DEM) of El Reventador Volcano. Contours are at 100 m  
 117 intervals, with bold contour lines every 500 m. The white polygons show the location of the 2002–2009 lava  
 118 flow field mapped by *Naranjo et al.* [2016]. The yellow polygon with white dashed outline shows the extent  
 119 of the 2011–2016 volcanic deposits. These deposits include lava flows mapped from Radarsat-2 amplitude  
 120 data (Fig. 4) and the area of topographic change between 9 September 2011 and 6 June 2014 from TanDEM-  
 121 X imagery (Fig. 5f). The yellow dot shows the location of the CONE seismic station, used by IG-EPN to  
 122 detect explosions at El Reventador. b) Location of El Reventador within Ecuador. c), d) Cumulative height  
 123 change of Phases A–E derived from TanDEM-X radar images. The topographic change is relative to the  
 124 SRTM DEM. Negative elevation changes near the summit in c) were caused by the removal of material during  
 125 the paroxysmal sub-plinian eruption on 3 November 2002 [*Hall et al.*, 2004]. This summit crater was almost  
 126 completely filled by new lava erupted during Phase E (d).



145 were separated by 18–24 months of quiescence (Fig. 2a; Table 3 of *Naranjo et al.* [2016]).  
 146 They estimated total lava volumes of  $90\text{M} \pm 37\text{M} \text{ m}^3$  from field measurements, and  $75\text{M}$   
 147  $\pm 24\text{M} \text{ m}^3$  from satellite remote sensing data. Based on visual, seismic and thermal obser-  
 148 vations of when lava flows are active, they present an average extrusion rate of  $8.9 \pm 3.7$   
 149  $\text{m}^3\text{s}^{-1}$  for periods of lava extrusion. The long-term time-averaged discharge rate (including  
 150 periods of repose) for Phases A–D was  $0.33 \pm 0.13 \text{ m}^3\text{s}^{-1}$  (Fig. 1).

151 Based on satellite thermal observations from the MODVOLC algorithm, Phase E  
 152 of the eruption at El Reventador began on 9 February 2012, following 23 months of mi-  
 153 nor activity [*Wright*, 2016]. Phase E was preceded by at least 8 months of growth of a  
 154 small lava dome at the summit of El Reventador [*Global Volcanism Program*, 2012]. The  
 155 first year of Phase E was characterised by mostly extrusive activity, followed by a step-  
 156 change in late 2012 or early 2013 to extrusive activity accompanied by numerous minor  
 157 explosions that were detected by the CONE seismic station on the northeast flank of El  
 158 Reventador (Fig. 2). Due to periods of intermittent failure of the CONE station, the explo-  
 159 sion record between 2012 and 2016 is incomplete. Phase E has lasted significantly longer  
 160 than previous eruptive phases, and is still ongoing as of June 2017. In this study, we fo-  
 161 cus on the time-averaged lava extrusion rate during Phase E, for which there exists a good  
 162 archive of radar satellite imagery.

### 163 **3 Surface morphology**

164 There are two approaches to measuring lava extrusion rate: instantaneous and time-  
 165 averaged. The first method records the instantaneous extrusion rate by observing the flux  
 166 of lava out of a volcano or vent at a particular time, and requires specific conditions in  
 167 the field, such as the ability to measure the velocity of lava flowing in an open channel  
 168 or tube of known dimension [e.g. *Harris et al.*, 2007]. The second approach involves mea-  
 169 suring the time-averaged discharge rate, which is the change in erupted volume averaged  
 170 over a given time period. Volume change at a volcano can be measured by comparing  
 171 the difference in topographic surface in between two digital elevation models (DEMs)  
 172 acquired at different times [e.g. *Wadge*, 1983; *Wadge et al.*, 2006a; *Harris et al.*, 2007;  
 173 *Ebmeier et al.*, 2012; *Xu and Jónsson*, 2014; *Poland*, 2014; *Albino et al.*, 2015; *Kubanek*  
 174 *et al.*, 2015; *Arnold et al.*, 2016; *Bagnardi et al.*, 2016]. The time-averaged discharge rate  
 175 is the sum of every pixel elevation difference, multiplied by the area of a raster grid cell,  
 176 divided by the time period between DEM acquisitions.



Recent advances in remote sensing have provided numerous techniques for generating DEMs, which can be used to build up a time series of topographic change at active volcanoes [Harris *et al.*, 2007; Schilling *et al.*, 2008; Diefenbach *et al.*, 2013; Cashman *et al.*, 2013; Pinel *et al.*, 2014; Wadge *et al.*, 2014b; Jones *et al.*, 2015; Bagnardi *et al.*, 2016]. Satellite radar is especially well suited to making repeat measurements of active volcanoes as it can cover a swath of 10–350 km at spatial resolutions of 1–10 m and repeat times of days to weeks, even at night or during cloudy conditions. [Wadge *et al.*, 2006b; Pinel *et al.*, 2014].

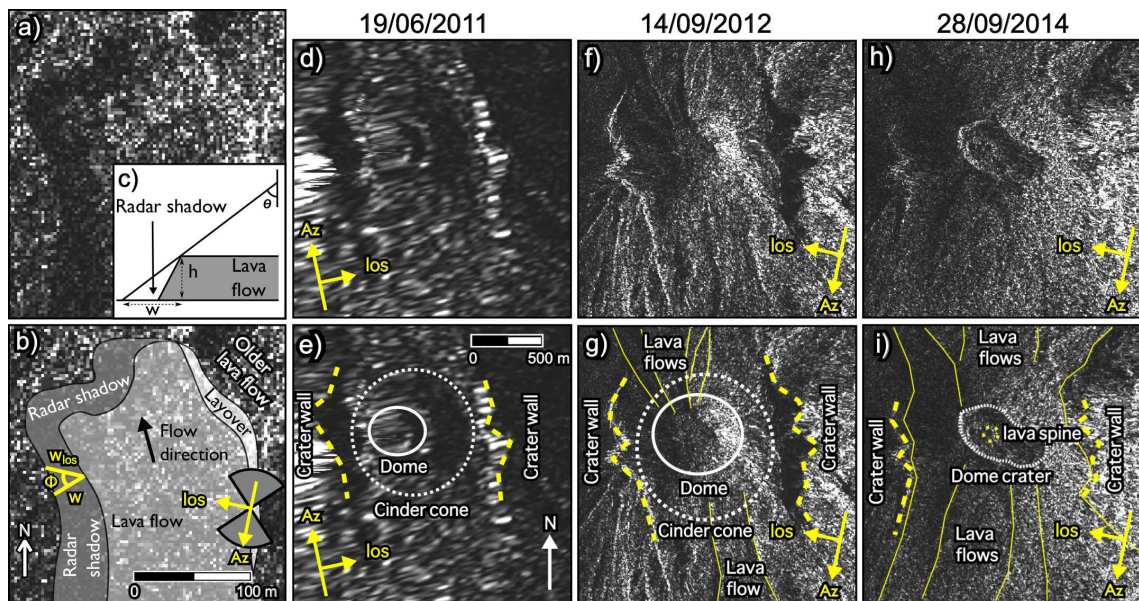
### 3.1 Radar methods

Variations in synthetic aperture radar (SAR) amplitude, caused by changes in surface roughness due to the emplacement of new volcanic deposits, can be used to map the extent of new lava flows [Wadge *et al.*, 2011; Dieterich *et al.*, 2012]. Where the edges of lava flows are steeper than the radar incidence angle, the lava flow will cast a shadow from which no signal is returned to the satellite. The width of this radar shadow is proportional to the height of the object casting it, so can be used to measure the thickness of steep sided lava flows (Fig. 3) using

$$h = \frac{w_{los} \cos \phi}{\tan \theta} \quad (1)$$

where  $h$  is the flow height,  $w_{los}$  is the shadow width in the radar line-of-sight direction, and  $\phi$  is the angle between the radar line-of-sight direction and the line perpendicular to the lava flow edge and  $\theta$  is the radar incidence angle. This technique only works on flow edges which are orientated within  $\sim 45^\circ$  of the satellite's direction of travel, in this case, a bearing of  $147\text{--}237^\circ$  for descending Radarsat-2 data at equatorial latitudes (grey rose diagram on Fig. 3b) [Wadge *et al.*, 2011]. Radar shadow thickness measurements can be used to estimate extruded lava volumes by assuming that lava flow thicknesses are constant across the whole flow and multiplying the thickness by the planimetric area of the flow.

The phase return of the radar signal can also be used to measure topography. For two satellites separated by a known distance, the difference in radar path length to the surface results in a phase difference in the interferogram formed between the image recorded



185 **Figure 3.** a) Radarsat-2 amplitude image of a lava flow which flowed from south to north on the northern  
 186 flank of El Reventador. b) Annotated amplitude image. The polygons give the extent of the flow, with the  
 187 radar shadow to the west in dark-grey and foreshortening and layover on eastern slopes facing the satellite  
 188 in white. The truncated shadow cast by an older lava flow is visible in the northeast of the image.  $Az$  is the  
 189 azimuth of the satellite direction of travel;  $los$  is the direction of radar line-of-sight;  $w_{los}$  is the width of the  
 190 shadow measured in the satellite look direction;  $\phi$  is the angle between  $w$  and  $w_{los}$ . The grey rose diagram  
 191 shows the range of flow edge orientations which can be measured using the shadow method. c) Schematic  
 192 representation of the radar shadow method for measuring lava flow thickness.  $w$  is the width of the radar  
 193 shadow, perpendicular to the flow edge;  $\theta$  is the radar incidence angle;  $h$  is the height of the lava flow. d), e),  
 194 f), g), h), i) Radarsat 2 amplitude images of the El Reventador lava dome, growing at the top of a cinder cone  
 195 within a summit crater. d) and e) were acquired in beam mode Wide 3, f), g), h), and i) were acquired in beam  
 196 mode Ultrafine25 Wide 2. The extent of the dome is given by the solid white ellipse, the cinder cone by the  
 197 dotted white ellipse and the yellow dashed lines show the position of the west and east walls of the summit  
 198 crater, which is breached to the north and south. Thin solid yellow lines in e) g) and i) highlight the edges of  
 199 emplaced lava flows. h) and i) show a  $\sim 24$  m diameter lava spine extruded from the centre of an explosion  
 200 crater at the summit of the lava dome.

222 at each satellite. The topography associated with the phase difference [Massonnet and  
223 Feigl, 1998, e.g.] is given by

$$224 \quad z = \frac{r\lambda \sin \theta}{4\pi B_{\text{perp}}} \Phi_{\text{topo}} \quad (2)$$

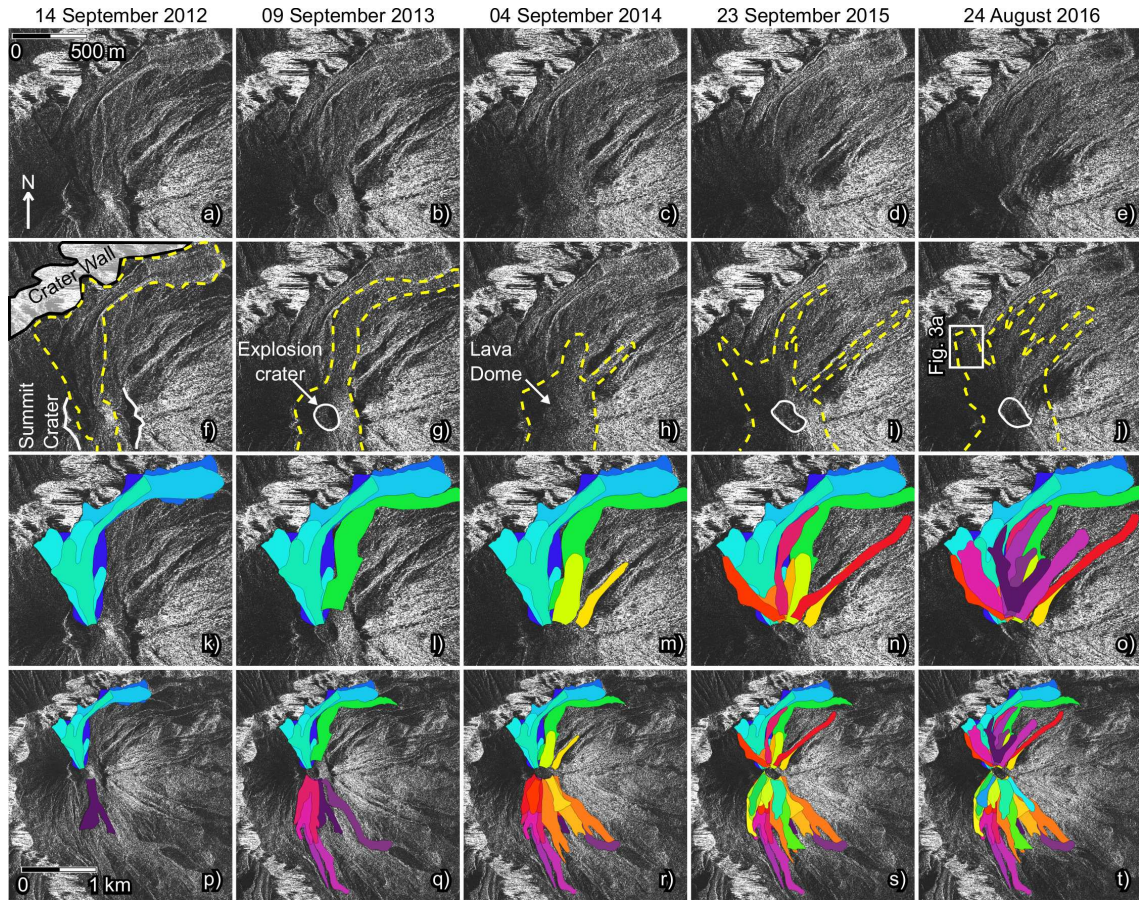
225 where  $z$  is the height,  $r$  is the range from the satellite to the ground surface,  $\theta$  is  
226 the incidence angle,  $B_{\text{perp}}$ , the effective baseline is half the perpendicular distance be-  
227 tween the two satellites [e.g. Kubanek *et al.*, 2015], and  $\Phi_{\text{topo}}$  is the topographic phase.  
228 For bistatic systems, where one sensor transmits and two sensors simultaneously record  
229 the same reflected signal, the phase contributions in an interferogram are due to the topog-  
230 raphy, the curvature of the earth, and noise [e.g. Poland, 2014; Kubanek *et al.*, 2015]. The  
231 contribution from the earth's curvature can be modelled and removed, leaving a phase dif-  
232 ference which is only due to topographic height and noise, without any atmospheric phase  
233 contribution.

### 234 **3.2 Data and processing**

235 We use satellite radar data from September 2011 to August 2016 to track changes  
236 in surface morphology associated with the eruption of El Reventador. A total of 32 im-  
237 ages from the Canadian Space Agency (CSA) satellite Radarsat-2 and 9 images from  
238 the Deutsches Zentrum für Luft- und Raumfahrt e. V. (DLR; German Space Agency)  
239 TanDEM-X mission were used. The satellite images are separated by time intervals rang-  
240 ing from 11 days to 10 months. Radarsat-2 images from two different beam modes are  
241 used — 25 acquired in ultrafine wide mode, and 7 in wide mode (Supplementary Table  
242 S2). TanDEM-X acquisitions over El Reventador ended in July 2014, while Radarsat-2  
243 images cover the whole period of interest from June 2011 until August 2016.

244 The TanDEM-X satellite pair operate in bistatic imaging mode, so the radar phase  
245 can be used to directly estimate the topography (equation 2). In contrast, repeat-pass Radarsat-  
246 2 interferograms contain phase contributions due to changes in atmospheric water vapour  
247 and ground deformation between image acquisitions, which make measurements of topo-  
248 graphic change more difficult. We use the amplitude component of the Radarsat-2 image  
249 to estimate the thickness of lava flows which have been active since the previous image  
250 acquisition (equation 1), and the phase component to check for ground deformation at El  
251 Reventador.





252 **Figure 4.** Extent of the lava flow field at El Reventador active between 6 March 2012 and 24 August 2016  
 253 mapped from Radarsat-2 amplitude imagery. **a), b), c), d), e)** Radarsat-2 amplitude image of the summit  
 254 and north flank of the active cone. Lighter colours indicate higher amplitude backscatter from slopes facing  
 255 towards the ~ west looking satellite, while darker areas are slopes facing away from the satellite. **f), g), h),**  
 256 **i), j)** Yellow dashed lines outline the area of the lava flow field which has changed since the previous image  
 257 due to new lava extrusion (**f)** is the change from the first Radarsat-2 acquisition on 6 March 2012). The solid  
 258 white lines in **f)** show the rim of the summit crater, which formed during the 3 November 2002 paroxysmal  
 259 eruption. The white box in **j)** show the location of Fig. 3a. White polygons in **g), h),** and **j)** outline craters  
 260 in the summit lava dome formed by Strombolian explosions. **k), l), m), n), o)** Cumulative lava flow field on  
 261 the north flank of El Reventador. Individual lava flows are plotted with younger flows superimposed on older  
 262 solidified flows. **p), q), r), s), t)** Cumulative lava flow field at El Reventador between 2012 and 2016. Colors  
 263 are schematic to differentiate separate lava flows.

264 We processed InSAR data using the Interferometric SAR Processor of the GAMMA  
265 software package [Werner *et al.*, 2000]. Bistatic TanDEM-X data were processed to con-  
266 struct DEMs of El Reventador at the time of each image acquisition using the methods  
267 described below.

268 Images were multi-looked with 4 looks in range and azimuth directions to reduce  
269 phase noise. The Shuttle Radar Topography Mission (SRTM) 30 m DEM, acquired in  
270 February 2000, was linearly oversampled to 6 m and used as the reference DEM to es-  
271 timate the topographic phase contribution for each interferogram (equation 2). We find no  
272 evidence of artefacts associated with the oversampling in the residual topographic phase.  
273 Changes in topography since 2000 due to the eruption of El Reventador, which began in  
274 2002, appear as residual phase contributions. For each interferogram, the vertical elevation  
275 change,  $z$ , can be calculated using equation 2. Adding this height change to the SRTM  
276 topography gives a new DEM for each satellite acquisition. The DEMs produced from the  
277 TanDEM-X imagery have a pixel spacing of 6 m. The difference in elevation between two  
278 DEMs multiplied by the area of a single pixel ( $36 \text{ m}^2$ ) gives the bulk volume change due  
279 to the eruption between the two dates.

280 The amplitude component of each Radarsat-2 image was geocoded from radar view-  
281 ing geometry into latitude and longitude coordinates by cross correlation with a simulated  
282 amplitude image generated from a DEM, in order to map lava flow extents and estimate  
283 flow thicknesses (Equation 1). Radarsat-2 amplitude images were processed at full reso-  
284 lution in order to preserve the minimum horizontal pixel spacing for measuring shadow  
285 widths. In order to minimise horizontal offsets in the amplitude imagery, all images were  
286 coregistered to a single master image and geocoded to the same DEM, which was gener-  
287 ated from the TanDEM-X acquisition on the 9th September 2011. The geocoded ampli-  
288 tude images have a horizontal pixel spacing of 2.5 m, and were imported into the QGIS  
289 software package for analysis.

290 For each time step, we identified lava flows which had been active since the preced-  
291 ing image acquisition through visual comparison to the previous and subsequent images.  
292 Flow outlines were mapped, and the planar area of each flow was measured. Where pos-  
293 sible, radar shadow widths were measured every 100 m downslope along each active lava  
294 flow and converted to thickness estimates using equation 1. The mean flow thickness was

295 then multiplied by the flow area to give the bulk volume of each lava flow, and a total  
296 bulk lava volume for every time step.

297 For both the TanDEM-X and Radarsat-2 data, bulk volume estimates are converted  
298 to a dense rock equivalent (DRE) volume. We assume the lavas erupted between 2012  
299 and 2014 are petrologically similar to those erupted between 2002 and 2009, which were  
300 found to have a vesicularity of  $\sim 20\%$  [Naranjo, 2013]. We therefore multiply our bulk  
301 volume measurements by a factor of 0.8 to estimate DRE volumes.

### 302 3.3 Error estimates

303 Both methods of estimating lava flow volume have associated uncertainties. The am-  
304 plitude estimates assume that lava flow thicknesses measured at the edge of the flow are  
305 representative of the entire flow. Equation 1 assumes that the lava flow is travelling on flat  
306 surface, which is not the case at El Reventador, where flows are descending an approx-  
307 imately conical edifice with numerous, radially oriented, eroded gulleys and a complex  
308 pre-existing lava flow field. In places where multiple flows are active between two im-  
309 age acquisitions, flows active earlier in this period may be partially or wholly buried by  
310 younger flows. The area of the buried portion of the flow therefore has to be estimated,  
311 which adds additional uncertainty into the flow volume measurement. We assume shadow  
312 width measurements may be inaccurate by up to two pixels (5 m), which corresponds to a  
313 height error of between 2.9 and 4.5 m depending on the orientation of the flow edge rel-  
314 ative to the satellite look direction (Equation 1). For flows where shadow measurements  
315 were possible along the whole length of the flow, the standard deviation in height mea-  
316 surements ranges between 1.5 m and 12.9 m, with a strong mode between 2 m and 3 m.  
317 We also assume flow area measurements are uncertain by variations in flow edge location  
318 of up to 5 m. Summing these errors for each time step give uncertainties in the amplitude  
319 volumes estimate of 15–40 %, similar to uncertainties of 5–35 % estimated by Naranjo  
320 *et al.* [2016] for field measurements of lava flow volume at El Reventador between 2002  
321 and 2009.

322 The noise component of the topographic change derived from TanDEM-X phase  
323 measurements can be estimated by looking at the variation of measured height change  
324 in an area known to not be significantly affected by the eruption, and assumed to be at a  
325 constant elevation in all images. We use a 100 by 100 pixel box east of the summit within

326 the caldera as a reference area to give an estimate of the relative errors in the TanDEM-  
 327 X derived DEMs. The reference area contains lava flows that were emplaced before the  
 328 onset of the most recent eruptive period in 2002 and are not likely to be subsiding. For El  
 329 Reventador, these errors are approximately  $\pm 0.7$  m for each pixel, therefore we expect to  
 330 be able to detect lava flows or pyroclastic deposits with a minimum thickness of 1 m. For  
 331 each TanDEM-X derived volume change estimate, the cumulative errors from summing  
 332 the uncertainty for each pixel give total uncertainties of 5–20 %, approximately half the  
 333 uncertainty associated with the shadow method.

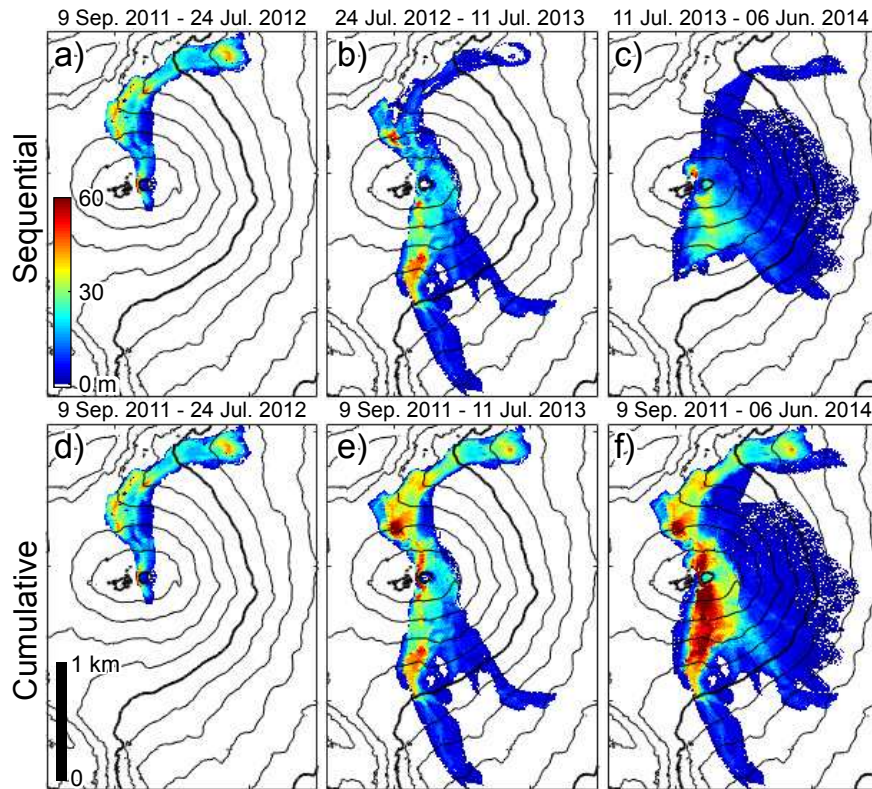
### 334 **3.4 Lava volume**

335 Using Radarsat-2 amplitude imagery, we map 39 discrete lava flows between Febru-  
 336 ary 2012 and August 2016, which all appear to have originate from the summit lava dome;  
 337 18 of which descended down the north flank and 21 down the south flank (Fig. 4, Supple-  
 338 mentary Table S4). At least one active flow is present in 24 of the 25 scenes (Supplemen-  
 339 tary Table S4) and all of the scenes show changes in the lava dome and summit crater  
 340 morphology, showing that activity at El Reventador is apparently continuous when ob-  
 341 served at intervals of 24 days. The total bulk volume of extruded lava flows during Phase  
 342 E from 9 February 2012 until 24 August 2016 measured by Radarsat-2 amplitude imagery  
 343 is  $56.0\text{M} \pm 3.1\text{M m}^3$ , which gives a dense rock equivalent (DRE) of  $44.8\text{M} \pm 2.5\text{M m}^3$   
 344 using a vesicularity of 20 % [Naranjo, 2013]. Lava dome volumes are over an order of  
 345 magnitude less than lava flow volumes, and are not included in this estimate (Section 3.5,  
 346 Supplementary Tables S4 and S5).

347 Topographic change maps derived from TanDEM-X imagery show surface elevation  
 348 changes of up to 80 m between September 2011 and June 2014 (Fig. 5). The greatest cu-  
 349 mulative lava flow thicknesses are on the north and south flanks of El Reventador, within  
 350 1 km of the summit. The cumulative bulk volume difference for Phase E up to 6 June  
 351 2014 was  $33.3\text{M} \pm 1.5\text{M m}^3$  ( $26.7\text{M} \pm 1.2\text{M m}^3$  DRE).

356 Radarsat-2 amplitude imagery and TanDEM-X phase observations both show the  
 357 cumulative volume of lava erupted at El Reventador increased throughout 2012 to 2016,  
 358 with no significant pauses in extrusion (Fig. 6a). Lava volumes measured by the radar  
 359 shadow method are in good agreements with the total volume change measured by DEM  
 360 differencing for the two year period where both data are available (9 September 2011 to





352 **Figure 5.** Topographic height change due to lava extrusion at El Reventador from DEMs constructed  
 353 from TanDEM-X imagery. **a), b), c)** Sequential elevation difference maps each spanning approximately one  
 354 year. **d), e), f)** Cumulative height change during Phase E of activity at El Reventador, relative to the earliest  
 355 available TanDEM-X acquisition on 9 September 2011.

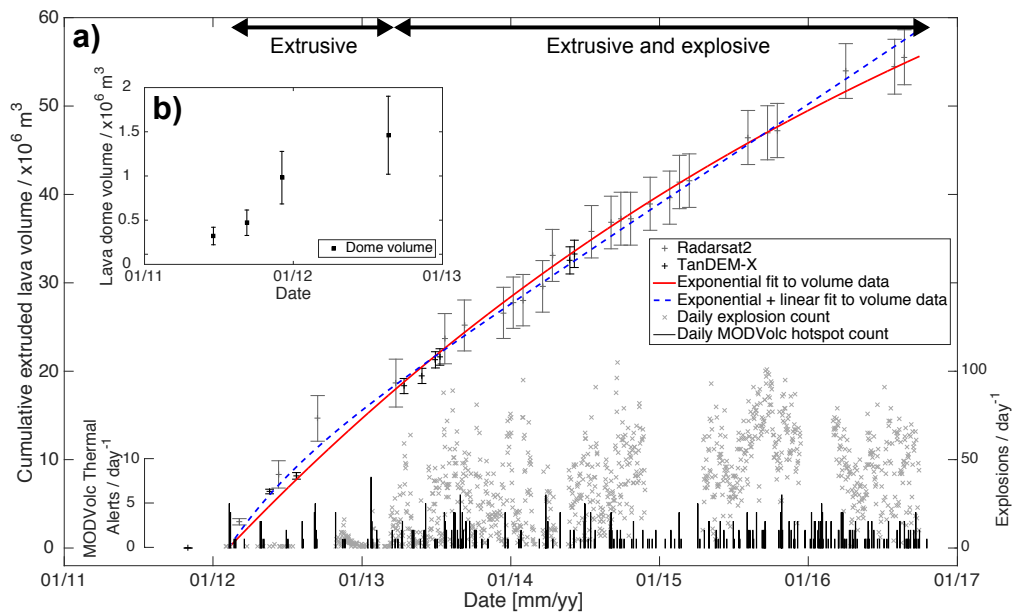
361 6 June 2014) — 33.1–35.8M m<sup>3</sup> from the shadow method compared to 33.3M m<sup>3</sup> from  
 362 DEM differencing. The similarity between results from the different methods suggests that  
 363 the erupted products are volumetrically mostly lava flows, with little contribution from  
 364 ash or pyroclastic deposits (which do not have steep sides and are therefore difficult to  
 365 measure with the shadow method).

366 The overall trend of the volume increase through time can be fit by an exponential  
 367 with the form  $V = A(1 - e^{-Bt})$  (red line in Fig. 6a, Table 1, equation 3), or with the form  
 368  $V = A(1 - e^{-Bt}) + Ct$  (blue line in Fig. 6a, Table 1, equation 9), where  $A$ ,  $B$  and  $C$  are  
 369 all constants. The first equation is consistent with a closed depressurising magma reser-  
 370 voir without magma recharge, while the second equation represents the case of an open  
 371 depressurising magma reservoir being resupplied at a constant volume flux  $C$  [Huppert  
 372 and Woods, 2002; Segall, 2013]. Both equations fit the data with a coefficient of determi-  
 373 nation,  $R^2 > 0.99$  and similar root-mean-square error (RMSE) of 0.29M m<sup>3</sup> with recharge  
 374 and 0.34M m<sup>3</sup> without.

375 The bulk time-averaged discharge rate derived from the gradient of the best expo-  
 376 nential fit (without recharge) gradually decreases throughout the observation period from  
 377 approximately 0.47 m<sup>3</sup>s<sup>-1</sup> at the beginning of extrusion in February 2012 to 0.28 m<sup>3</sup>s<sup>-1</sup>  
 378 at the end of the observation period in August 2016. Alternatively, assuming constant  
 379 magma recharge, the best fitting initial bulk time-averaged discharge rate was 0.77 m<sup>3</sup>s<sup>-1</sup>  
 380 in February 2012 and decreased more rapidly to 0.41 m<sup>3</sup>s<sup>-1</sup> after one year, and reached  
 381 the recharge rate,  $C$ , of 0.36 m<sup>3</sup>s<sup>-1</sup> by early 2014. In contrast, the best fitting linear gra-  
 382 dient, without an exponential component, has a bulk rate of 0.44 m<sup>3</sup>s<sup>-1</sup>. This linear rate  
 383 consistently underestimates the cumulative erupted volumes in 2012 to 2014, while over-  
 384 estimating the total volume throughout 2015 and 2016. Physics-based interpretations of  
 385 these observations are discussed in section 5.

### 395 **3.5 Dome growth and crater morphology**

396 At the start of our observation period in June 2011, El Reventador had a small lava  
 397 dome that was growing at the top of a cinder cone that formed during 2009, located inside  
 398 the summit crater formed by the 3 November 2002 paroxysmal explosion Fig. 3; [*Global*  
 399 *Volcanism Program*, 2012]), which we estimate to be ~ 50 m deep (Fig. 2c). From the  
 400 Radarsat-2 amplitude image acquired on 19 June 2011 (Fig. 3d and e), we observe the



386 **Figure 6.** **a)** Cumulative bulk volume of extruded lava at El Reventador. The mid-grey points are estimated  
 387 from Radarsat-2 shadow measurements. Black points are TanDEM-X phase measurements. The solid red  
 388 and dashed blue lines give best fitting curves to the volume data. Pale-grey crosses show the daily explosion  
 389 count, recorded by the CONE seismic station located within the El Reventador caldera. Gaps in the explo-  
 390 sivity record, for example in late 2012, 2014, early 2015 and early 2016, were due to intermittent failure of  
 391 the CONE seismic station and do not indicate periods of no explosive activity. Vertical black bars show the  
 392 number of daily hotspot pixels detected by the MODVolc algorithm. **b)** Bulk volume of the lava dome at the  
 393 summit of El Reventador, assuming the dome is a half ellipsoid. After 2013, explosions repeatedly remove  
 394 part of the dome, hindering volume measurements.

401 lava dome to be elliptical and measure the length of the semi-major and semi-minor axes  
 402 (Supplementary Table S5). We also use the shadow method to estimate the dome height  
 403 and the depth of the summit crater which was  $\sim 50$  m on 19 June 2011. We observe ex-  
 404 pansion of the dome through June to December 2011, consistent with aerial and field ob-  
 405 servations, which found a broadening of the dome between July 2011 and January 2012  
 406 [*Global Volcanism Program*, 2012]. After the start of lava flow extrusion in February  
 407 2012, the dome became partially covered by lava flows, which appear to originate from  
 408 the summit of the dome, making size and shape difficult to determine, however we are  
 409 able to estimate the dome dimensions on 14 September 2012 (Supplementary Table S5).

410 We treat the dome as the upper half of an oblate ellipsoid such that the bulk volume  
 411  $V = 2\pi abc/3$ , where  $a$  is the semi-major half axis,  $b$  is the semi-minor half axis, and  $c$   
 412 is the dome height (Fig. 6b). These dimensions yield a bulk dome volume of  $0.33\text{M m}^3$   
 413 in June 2011, growing to  $0.48\text{M m}^3$  in September and  $0.99\text{M m}^3$  by the end of December  
 414 2011. The bulk time-averaged discharge rate for June to September 2011 was therefore  
 415  $0.021 \text{ m}^3\text{s}^{-1}$ , rising to  $0.069 \text{ m}^3\text{s}^{-1}$  for September to December 2011, significantly less  
 416 than the time-averaged rate after lava flow extrusion began in February 2012 ( $0.47 \text{ m}^3\text{s}^{-1}$ ).  
 417 The volume of the dome increased to  $1.47\text{M m}^3$  by September 2012 at a rate of  $0.023$   
 418  $\text{m}^3\text{s}^{-1}$ , however the volume of lava flows extruded during this period was one order of  
 419 magnitude greater (Supplementary Table S4).

420 The SAR image on 25 March 2013 postdates the start of frequent minor explo-  
 421 sive activity that occurred in early 2013 at El Reventador. A 120 m diameter crater is  
 422 present at the centre of the lava dome, and talus deposits are visible within the 2002 sum-  
 423 mit crater, piling up against the east and west crater rims. In the 31 January 2014 SAR  
 424 image, pyroclastic deposits are visible in gullies on the east flank of El Reventador. These  
 425 deposits were not present on 7 January 2014, suggesting that in the intervening 24 days,  
 426 the base of the dome reached a height from which pyroclastic density currents were able  
 427 to overtop the east wall of the 2002 summit crater. Shadow measurements of the eastern  
 428 crater rim suggest up to 30 m of height change during this time period, although TanDEM-  
 429 X measurements suggest less than 20 m elevation change between 11 July 2013 and 6  
 430 June 2014 (Fig. 5c).

431 The dome morphology continued to change throughout 2013–2016, with a crater  
 432 present at the top of the lava dome in 20 out of 22 Radarsat-2 amplitude images after ex-

433 plosivity begins. In four of these images, there is a small area of paired radar layover and  
434 shadow, indicative of a feature with steep sides and without a flat top (Fig. 3h). These fea-  
435 tures are all located in approximately the same area within dome summit craters and are  
436 20–30 m in diameter and, from radar shadow widths, have a maximum height between  
437 14 and 19 m above the crater floor. We interpret these features as lava spines — solidi-  
438 fied lava that has been extruded out of a conduit by pressure from below, which were also  
439 observed at El Reventador between 2009 and 2012 [*Global Volcanism Program*, 2012].

440 From TanDEM-X derived DEMs, we estimate that between 9 September 2011 and  
441 6 June 2014, the average elevation of the lava dome increased by  $24 \pm 4$  m, while the dis-  
442 tribution of talus deposits was constrained by the 2002 summit crater rim and increased in  
443 mean thickness by  $59 \pm 11$  m west of the dome and  $39 \pm 2$  m to the east. We observe mi-  
444 nor negative topographic changes between some sequential TanDEM-X DEMs associated  
445 with crater formation at the summit of the lava dome, however this volume loss is negligi-  
446 ble compared to the overall volume increase. The largest volume removal we observe was  
447 between 28 May and 30 June 2013 with a volume decrease at the summit of  $\sim 0.15\text{M m}^3$ ,  
448 while the net volume increase (including lava flows) for the same period was  $\sim 1.8\text{M m}^3$ .

449 Radarsat-2 amplitude images from July 2014 to August 2016 show continued lava  
450 dome growth and talus build up against the 2002 summit crater walls, which by August  
451 2016 had been almost completely in-filled. Images acquired after January 2014 suffer  
452 from geometric distortion near the summit of the lava dome due to changes in elevation  
453 since the acquisition of the TanDEM-X DEM on 9 September 2011, which was used to  
454 geocode all the satellite data into a common geometry for flow identification and analysis.

## 455 **4 Ground deformation and modelling**

### 456 **4.1 Differential interferometry**

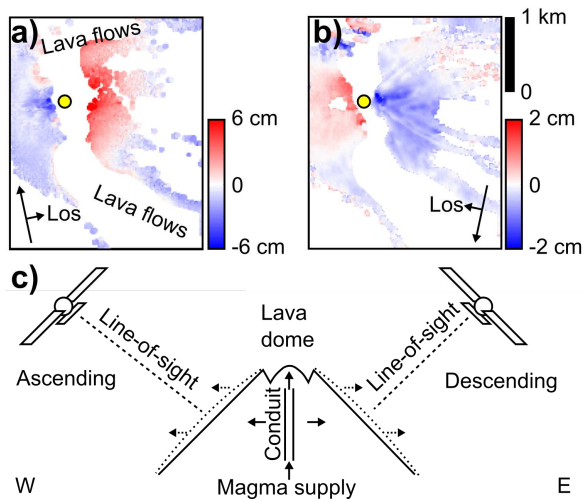
457 For both Radarsat-2 and TanDEM-X data, repeat-pass differential interferograms  
458 were constructed using GAMMA to measure ground deformation at El Reventador [e.g.  
459 *Massonnet and Feigl*, 1998; *Dzurisin*, 2003]. The topographic phase term was estimated  
460 using the 6 m DEM generated from earliest available TanDEM-X acquisition on the 9th  
461 September 2011. The interferograms were filtered using an adaptive density filter [*Gold-*  
462 *stein and Werner*, 1998], unwrapped using a minimum cost flow algorithm [*Werner et al.*,  
463 2002] and geocoded to the 2011 TanDEM-X DEM.

464 At El Reventador, loss of coherence is primarily caused by rapid vegetation growth  
465 in distal areas outside the recent lava flow field, and by resurfacing of the area proximal  
466 to the summit by lava flow extrusion, dome growth, rockfalls, and tephra and pyroclastic  
467 deposits [e.g. *Ebmeier et al.*, 2014]. Areas outside the  $6 \times 4$  km El Reventador crater are  
468 almost entirely incoherent, while recent less-vegetated lava flows within the crater, up to 4  
469 km from the active vent, are much more coherent. The flows show subsidence associated  
470 with cooling and compaction of the blocky lavas, a result previously observed in ALOS  
471 data from 2007–2011 [*Fournier et al.*, 2010; *Naranjo et al.*, 2016; *Morales Rivera et al.*,  
472 2016]. The combined effect of lava subsidence in the near-field and incoherence in the  
473 far-field masks almost all potential edifice-wide ground deformation due to magmatic or  
474 hydrothermal processes underneath El Reventador.

#### 475 **4.2 Dyke intrusion**

476 We observe one period of ground deformation that we attribute to subsurface mag-  
477 matic processes at El Reventador. The deformation is present in the ascending Radarsat-2  
478 interferogram between 9 March 2012 and 31 July 2012, and the descending interferogram  
479 spanning 6 March 2012 to 10 June 2012. In both interferograms, the deformation is lim-  
480 ited to the area near the summit of the stratocone, just outside of the 2002 eruption crater,  
481 and the east and west flanks have an opposite displacement direction in the satellite line-  
482 of-sight. The ascending scene shows the west flank moved towards the east looking satel-  
483 lite, with a maximum magnitude of  $\sim 2$  cm, while the east flank moved away from the  
484 satellite by up to 5 cm. In contrast, in the descending scene, the west flank has moved  
485 away from the west looking satellite by  $\sim 1$  cm and the east flank moved  $\sim 1.5$  cm to-  
486 ward the satellite (Fig. 7). These observations indicate motion is dominantly horizontal,  
487 where the east flank moves to the east and the west flank moves west, consistent with a  
488 dyke opening underneath the summit. We assume the deformation observed in both inter-  
489 ferograms happened simultaneously in a short duration event, and that this dyke opening  
490 event occurred between 9 March 2012 and 10 June 2012.

496 The direction, magnitude and spatial distribution of the deformation suggest that the  
497 source of the deformation is located underneath the summit of El Reventador, within the  
498 volcanic edifice. The shallow nature of the source, as demonstrated by the limited lateral  
499 extent of the deformation signal, suggests that the deformation is associated with the con-



491 **Figure 7.** **a)** Line-of-sight deformation (positive away from satellite, negative towards satellite) between  
 492 9 March 2012 and 31 July 2012 from ascending Radarsat-2 data. **b)** Line-of-sight deformation between 6  
 493 6 March 2012 and 10 June 2012. The yellow circle indicates the location of the lava dome. Recent lava flows  
 494 have been masked to remove deformation associated with subsidence. **c)** Schematic representation of the  
 495 deforming edifice and satellite viewing geometries.

500 duit supplying the eruption at the surface, and that the dyke or conduit expanded a few  
 501 weeks or months after lava flow extrusion began.

502 To investigate the geometry of this magmatic source for the March-June 2012 ground  
 503 deformation at El Reventador, we performed a joint inversion on the two interferograms in  
 504 which the deformation was observed using an elastic dislocation model (Supporting in-  
 505 formation, [Okada, 1985; Hooper *et al.*, 2013; González *et al.*, 2015]). The lowest misfit  
 506 model solution of this inversion is a small ( $100 \times 600$  m), shallow (base of dyke  $<1$  km  
 507 deep), vertical dyke oriented approximately north-south, opening by less than 1 m, and  
 508 with a volume change of  $\sim 10000$  m<sup>3</sup> (Fig. 8a). This solution is able to fit most of the  
 509 deformation signal in the descending interferogram, but with significant and spatially com-  
 510 plex residuals, and it substantially underestimates the magnitude of the deformation in the  
 511 ascending interferogram. The misfit between the data and models is likely due to multi-  
 512 ple factors that make the elastic half space approximation unrealistic, including: the large  
 513 ( $>1000$  m, Fig. 2a) topographic relief near the summit of El Reventador; the complex ge-  
 514 ometry of the volcanic edifice, lava, summit crater and lava flow field; and the likely non-



515 elastic rheology of the shallow subsurface due to a combination of shallow hydrothermal  
516 activity and thermal and mechanical relaxation.

517 Despite the substantial uncertainties associated with the modelling method, the max-  
518 imum intrusive volume change is still likely to be on the order of  $0.01\text{M m}^3$ , which is  
519 approximately two orders of magnitude less than the extrusive lava volume for the same  
520 time period ( $\sim 5\text{M m}^3$ ), and therefore makes a negligible contribution to the overall magma  
521 budget. However, the expansion of the conduit may have caused a higher magma flux to  
522 the surface, resulting in an increase of the lava extrusion rate in the following months of  
523 2012, as shown by the deviation of observed lava volumes from the best fitting exponen-  
524 tial trend in mid to late 2012 (Fig. 6a).

525 We do not find evidence for any other ground deformation episodes after the dyke  
526 opening in March to June 2012. Subsequent interferograms do not show a reversal of the  
527 deformation trend, suggesting that the pathway for magma to the surface remained open  
528 after June 2012. This conduit opening may explain the increased lava extrusion rate in  
529 June 2012 to March 2013, relative to the long term exponential trend. Conduit opening  
530 would increase the cross-sectional area of the conduit, and therefore the volume flux at  
531 a given magma ascent velocity. There may be a correlation between the conduit opening  
532 and the increase in explosivity in early 2013, however there is a 9-12 month lag between  
533 the deformation episode and the increase in explosive activity.

534 It is likely that there are shorter term deformation processes associated with the con-  
535 duit and lava dome at El Reventador, similar to those observed at Montserrat, Colima  
536 and Santiaguio [Voight *et al.*, 1998; Johnson *et al.*, 2008; Sanderson *et al.*, 2010; Walter  
537 *et al.*, 2013; Salzer *et al.*, 2014]. Seismic records indicate up to 50 explosions per day at  
538 El Reventador (Fig. 6a), giving an average repose period between explosions of  $\sim 30$  min-  
539 utes. Santiaguio volcano in Guatemala exhibits similar  $\sim 30$  minute period explosivity,  
540 which are accompanied by up to 50 cm of uplift of the dome surface 1-2 seconds before  
541 the explosions [Johnson *et al.*, 2008; Scharff *et al.*, 2012]. These transient processes oc-  
542 cur on much shorter timescales than the observation frequency of satellite InSAR, and are  
543 usually shallow and therefore only deform the area proximal to the active lava dome. De-  
544 formation observations within  $\sim 500$  m of the summit of El Reventador are impossible  
545 after September 2012 due to loss of coherence caused by resurfacing of the ground sur-

546 face by ashfall and pyroclastic deposits that were associated with the increase in explosive  
547 activity.

### 548 **4.3 Constraints on reservoir volume**

549 Interferograms from June 2012 onwards do not contain any evidence of magmatic  
550 deformation at El Reventador. If we assume a magma reservoir geometry and place rea-  
551 sonable bounds on its location, we can put a lower limit on the minimum possible volume  
552 change that we would be able to detect given the level of noise in sequential interfero-  
553 grams [e.g. *Ebmeier et al.*, 2013b]. We consider the simple case of a volume change in a  
554 ‘Mogi’ point source situated underneath the summit of El Reventador [*Mogi*, 1958]. We  
555 consider the difference expected line-of-sight deformation in the area between 1 km and  
556 2 km from the summit, which is mostly coherent in all interferograms. The average vari-  
557 ance in line-of-sight deformation across the 23 Radarsat 2 descending interferograms is  $\sim$   
558 3 mm, which we consider to be the detection threshold for magmatic deformation at El  
559 Reventador. For a given reservoir depth, we assume we would be able to detect a reser-  
560 voir volume change that resulted in 3 mm of line-of-sight range change at a horizontal  
561 distance of 1 km relative to at 2 km.

562 If we assume the 2012–2016 reservoir is at similar depths to the pre-2002 reservoir  
563 [7–12 km; *Samaniego et al.*, 2008; *Ridolfi et al.*, 2008], then the minimum volume change  
564 we would be able to detect is between 10M and 100M m<sup>3</sup> — a similar order of magni-  
565 tude to the  $44.8\text{M} \pm 2.5\text{M}$  m<sup>3</sup> DRE that was extruded during this time period.

## 566 **5 Models of the magmatic system**

567 Our data show eruption of lava at a slowly decreasing extrusion rate, with no sig-  
568 nificant detectable ground deformation. Here we introduce a simple physics-based model  
569 of a volcanic system and apply the model to our observations to attempt to constrain the  
570 physical characteristics of the magmatic system at El Reventador.

571 Physics-based volcano models provide a means of linking observations with un-  
572 derlying physical properties and processes [e.g. *Sparks and Aspinall*, 2004; *Costa et al.*,  
573 2007; *Anderson and Segall*, 2011; *Cashman and Sparks*, 2013; *Segall*, 2013; *Reverso et al.*,  
574 2014]. These models may be used in quantitative inverse procedures to constrain properties  
575 of the volcanic system [*Anderson and Segall*, 2013]. For example, a common observation

576 is that within an individual volcanic eruption, including Phase E at El Reventador, lava ex-  
 577 trusion rates are generally highest at the start of the eruption, and decrease through time  
 578 as the eruption progresses [e.g. *Wadge, 1981, 1983; Anderson and Segall, 2011; Hreinsdóttir*  
 579 *et al., 2014; Gudmundsson et al., 2016*]. This behaviour can be explained by balancing  
 580 mass flux out of a magma reservoir in a purely elastic medium with Newtonian flow along  
 581 a conduit, modelled as a cylindrical pipe, which gives the equations for exponential de-  
 582 cay of reservoir pressure change [e.g. *Scandone, 1979; Wadge, 1981; Huppert and Woods,*  
 583 *2002; Lu et al., 2003; Anderson and Segall, 2013; Hreinsdóttir et al., 2014*]:

$$584 \quad \Delta p(t) = (\bar{\rho}gL_c - p_{ch_0}) \left(1 - e^{-t/t_c}\right) \quad (3)$$

585 and the erupted volume:

$$586 \quad V_e(t) = V_0\bar{\beta}\Delta p(t) \quad (4)$$

587 as the eruption progresses [*Mastin et al., 2008; Anderson and Segall, 2011*]. In these equa-  
 588 tions,  $t$  is the time elapsed since the start of the eruption,  $\Delta p$  is the pressure change in the  
 589 reservoir, relative to the overpressure above magmastatic pressure at the start of the erup-  
 590 tion,  $p_{ch_0}$ .  $\bar{\rho}$  is the depth-averaged magma density along the conduit,  $g$  is the acceleration  
 591 due to gravity,  $L_c$  is the length of the conduit,  $V_0$  is the initial reservoir volume,  $\bar{\beta}$  is the  
 592 overall compressibility, which is the sum of  $\beta_m$ , the magma compressibility and  $\beta_{ch}$ , the  
 593 reservoir compressibility, and  $t_c$ , the time constant, is given by

$$594 \quad t_c = \frac{8\bar{\eta}V_0\bar{\beta}L_c}{\pi R^4} \quad (5)$$

595 where  $\bar{\eta}$  is the depth-averaged magma viscosity.

596 Ground deformation observations can be used to estimate reservoir location, ge-  
 597 ometry, and reservoir volume change or  $V\Delta p$  [e.g. *Mogi, 1958; Okada, 1985; McTigue,*  
 598 *1987; Yang et al., 1988*], and the erupted volume can be measured directly (Supplemen-  
 599 tary Table S1). Observations of ground deformation and erupted volume can therefore be  
 600 used in conjunction with equations 3, 4 and 5 along with information from other sources,  
 601 such as petrology, rock mechanics, and gas fluxes, to constrain reservoir parameters [e.g.  
 602 *Wadge, 1981; Melnik and Sparks, 2005; Costa et al., 2007; Mastin et al., 2008; Rivalta and*  
 603 *Segall, 2008; Anderson and Segall, 2013; Kozono et al., 2013; Hreinsdóttir et al., 2014; Re-*  
 604 *verso et al., 2014; Anderson and Poland, 2016*]. Here we present a physics-based model  
 605 based on a pressurised reservoir in an elastic upper crust linked to the surface by a con-  
 606 duit (Fig. 8a). We apply this model to our observations of erupted volume, temporal evo-

607 lution of eruption rate, and lack of long-term ground deformation at El Reventador to es-  
 608 timate magma reservoir properties that cannot be directly observed, such as reservoir vol-  
 609 ume, pressure change, magma supply rate, reservoir compressibility and volatile content  
 610 [e.g. *Mastin et al.*, 2008; *Anderson and Segall*, 2013; *Segall*, 2013; *Anderson and Poland*,  
 611 2016].

## 612 **5.1 Reservoir volume**

613 For short duration eruptions where there is negligible magma input, the initial vol-  
 614 ume of a magma reservoir  $V_0$  can be estimated from the erupted volume  $V_e$  by consider-  
 615 ing conservation of mass [*Anderson and Segall*, 2014],

$$616 \quad V_0 = -\frac{V_e}{\bar{\beta}\Delta p} \quad (6)$$

617 For simplicity, we assume that there is no density change in the magma between the reser-  
 618 voir and surface, and therefore the dense rock equivalent volume extruded at the surface  
 619 is the same as the volume that leaves the reservoir at the base of the conduit [e.g. *Gud-*  
 620 *mundsson*, 2016]. The error introduced by this assumption should be small compared to  
 621 the uncertainty in the parameters.

622 In order to estimate reservoir volume from the erupted volume, compressibility and  
 623 reservoir pressure change must be estimated (equation 6). Reservoir compressibility may  
 624 be constrained based on knowledge of reservoir geometry and host rock rigidity; magma  
 625 compressibility may be constrained a priori based on knowledge of typical magma prop-  
 626 erties in the crust, or else modelled directly as a function of the magma's various phases  
 627 [*Mastin et al.*, 2008; *Rivalta and Segall*, 2008; *Anderson and Segall*, 2011]. Additionally,  
 628 the ratio of reservoir and magma compressibility may be constrained a priori [*Anderson*  
 629 *and Poland*, 2016] based on observations at other eruptions [e.g. *McCormick-Kilbride*  
 630 *et al.*, 2016]. *Rivalta and Segall* [2008] define the ratio  $r_V$  between the erupted volume  
 631 and the change in volume within a magma reservoir as

$$632 \quad r_V = \frac{V_e}{\Delta V_{ch}} = 1 + \frac{\beta_m}{\beta_{ch}} = \frac{\beta_m + \beta_{ch}}{\beta_{ch}} \quad (7)$$

633 where  $\Delta V_{ch}$  is the absolute value of the volume change of the reservoir. Theoretical val-  
 634 ues for  $r_V$  for degassed magmas range between 1.05 and 9, however for volatile rich

635 magmas,  $r_V$  could be as high as 15 [Rivalta and Segall, 2008; McCormick-Kilbride *et al.*,  
636 2016].

637 We use the November 2002 paroxysmal eruption, which lasted approximately 45  
638 minutes, as a short duration eruption that can allow us to estimate the volume of the pre-  
639 2002 reservoir if we consider  $q_{in} = 0$  [Hall *et al.*, 2004]. The bulk volume of erupted  
640 ash and pyroclastic flows was estimated to be  $\sim 350\text{M m}^3$  [Hall *et al.*, 2004], which we  
641 convert to a DRE volume of  $150\text{M m}^3$  using densities for dense rock, pyroclastic flow de-  
642 posits and tephra deposits that we assume are representative of andesitic dome forming  
643 eruptions, taken from Soufrière Hills, Montserrat [Wadge *et al.*, 2010]. From comparison  
644 to other volatile rich systems, if we assume realistic upper bounds of  $1 \times 10^{-9} \text{ Pa}^{-1}$  for  $\bar{\beta}$   
645 and  $-20 \text{ MPa}$  for  $\Delta p$  (supporting information, [Woods and Huppert, 2003; Amoroso and  
646 Crescentini, 2009; Gudmundsson, 2016]), then  $V_0$  must be greater than  $7.5 \text{ km}^3$ . Alter-  
647 natively if we estimate upper bounds of  $2.25 \times 10^{-9} \text{ Pa}^{-1}$  for  $\bar{\beta}$  by using equation 7 and  
648 taking a maximum value of  $1.5 \times 10^{-10} \text{ Pa}^{-1}$  for  $\beta_{ch}$  and 15 for  $r_V$  [Rivalta and Segall,  
649 2008], then equation 6 gives  $V_0 \geq 3.3 \text{ km}^3$ . The upper limit of the reservoir volume is  
650 poorly constrained, however it is unlikely to be larger than approximately  $150 \text{ km}^3$  [Gud-  
651 mundsson, 2016].

652 The lack of deformation at El Reventador between 2012 and 2016 does not yield  
653 any additional constraints on reservoir volume, since  $\Delta V_{ch}$  is *a priori* almost certainly  
654 less than  $V_e$  (Section 4, [Rivalta and Segall, 2008; McCormick-Kilbride *et al.*, 2016]). We  
655 therefore consider it reasonable to assume that the current reservoir has approximately the  
656 same volume as the 2002 reservoir, since the  $150\text{M m}^3$  erupted in 2002 represents at most  
657 5 % of the total reservoir volume, which has to be greater than  $\sim 3 \text{ km}^3$  (Supporting in-  
658 formation). We therefore assume the current magma reservoir has a volume greater than 3  
659  $\text{km}^3$  with a poorly constrained upper limit.

## 660 5.2 Temporal evolution of extrusion rate

661 Considering the temporal evolution of the erupted volume allows us to constrain  
662 additional parameters of the magmatic system [e.g. Anderson and Segall, 2011]. If we  
663 model the reservoir recharge as time-constant, then following Huppert and Woods [2002]  
664 the change in reservoir pressure can be modelled by

$$\Delta p_{ch}(t) = -\left(p_{ch_0} - \frac{q_{in}t_c}{V_0\bar{\beta}}\right)\left(1 - e^{-t/t_c}\right) + \frac{q_{in}t}{V_0\bar{\beta}} \quad (8)$$

and the erupted volume by

$$V_e(t) = \left(V_0\bar{\beta}p_{ch_0} - q_{in}t_c\right)\left(1 - e^{-t/t_c}\right) + q_{in}t \quad (9)$$

Equation 9 shows that for time-constant input flux, the erupted volume flux ( $q_{out} \equiv dV_e/dt$ ) tends to the linear gradient  $q_{in}$  as  $t \rightarrow \infty$ . If  $q_{in} = 0$  then equation 9 simplifies to the case for a closed system given by equation 4.

If we approximate the conduit as an elliptical pipe, then time constant of the exponential decay is given by

$$t_c = \frac{4\bar{\eta}(a^2 + b^2)V_0\bar{\beta}L_c}{\pi(ab)^3} \quad (10)$$

which simplifies to the case of a cylindrical pipe, equation 5, where  $a = b = R$  [e.g. *Anderson and Segall, 2011; Hreinsdóttir et al., 2014*]. The derivations for equations 8–10 are given in the supporting information.

If El Reventador behaves as a closed system ( $q_{in} = 0$ ), the time constant of the eruption has 6 unknowns that trade off against each other (equation 10), therefore it is difficult to estimate any one parameter directly. Including a constant rate of magma supply adds an additional term for  $q_{in}$  that is independent of the time constant, but will trade off against it (equation 9). We are able to make measurements of  $\Delta V_e(t)$  from our satellite radar observations, and by fitting equations 4 and 9 to our results we can attempt to distinguish between a closed reservoir with no magma recharge or an open reservoir with recharge as potential models for the eruptive behaviour at El Reventador. By calculating  $t_c$  from the fit to the data and considering sensible limits of  $a$ ,  $b$ ,  $\bar{\beta}$ ,  $\bar{\eta}$ ,  $V_0$  and  $L_c$  (supporting information), we can investigate how these parameters trade off against each other and estimate likely values of each.

We estimate the best fitting model parameters for equation 9 using a non-linear least-squares method, evaluated with a trust-region algorithm using the MATLAB curve-fitting toolbox. We can assess the relative fit of the open and closed system models by comparing how the misfit between the data and model changes as  $q_{in}$  increases from 0. Fig. 8d shows the root mean square error (RMSE) between the extruded volume data for

Phase E and the best fit to equation 9 as  $q_{in}$  changes. We find that the misfit at the best fitting solution ( $0.29 \pm 0.01 \text{ m}^3\text{s}^{-1}$  DRE) is only slightly lower than the misfit at lower influx rates, including the closed system model, since  $q_{in}$  and  $t_c$  trade off against each other (equation 9, Fig. 8c). We are therefore able to place only an upper limit on the recharge rate at El Reventador, which we find to be  $0.35 \text{ m}^3\text{s}^{-1}$  DRE. This upper limit corresponds to the best fitting linear rate to the data (i.e.  $t_c = 0$ ). The misfit with the data increases significantly at higher constant recharge rates (Fig. 8b and c) and therefore this upper limit of the recharge rate is well constrained.

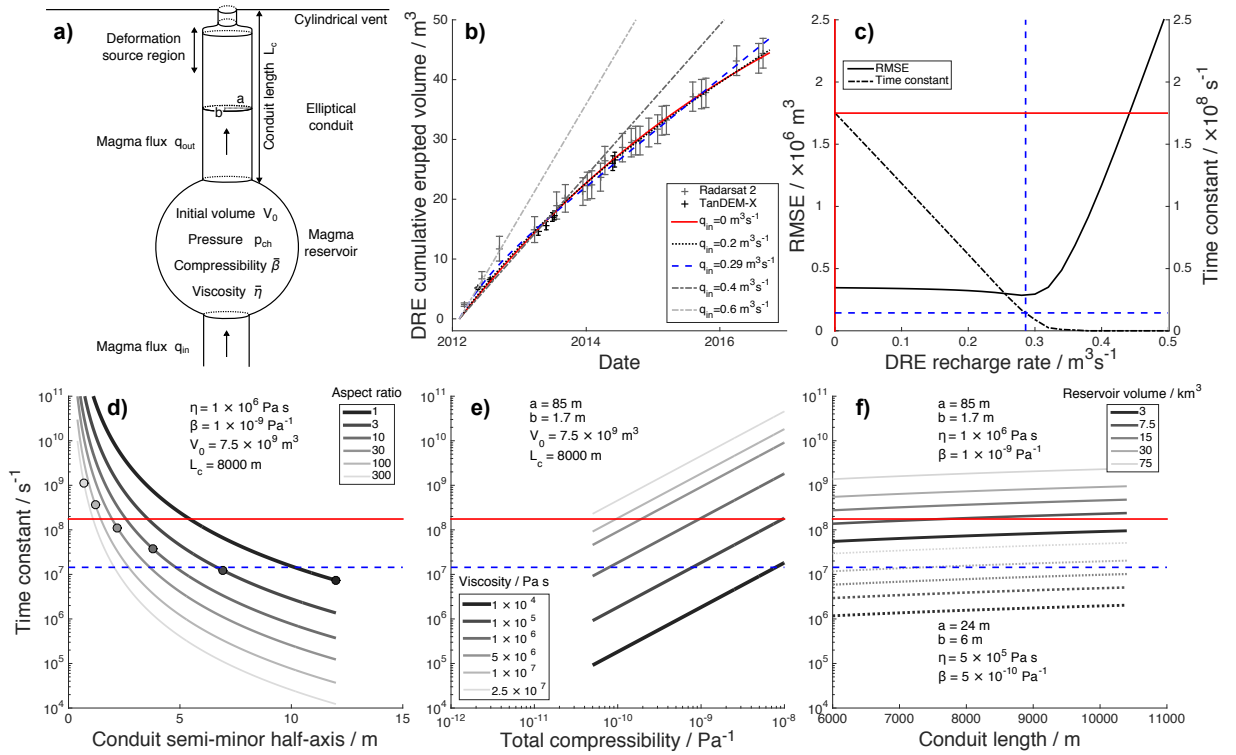
### 5.2.1 Temporal evolution of a closed system

If we first consider the magma reservoir at El Reventador to be a closed system with no magma recharge during Phase E ( $q_{in} = 0$ ) then this approach yields a good fit to the data (red line in Fig. 6a) with a time constant  $t_c$  of 2000 days, with 95 % confidence limits between 1700 and 2600 days. Using equation 10 we can consider how conduit dimensions  $a$  and  $b$ , effective viscosity  $\bar{\eta}$ , compressibility  $\bar{\beta}$ , conduit length  $L_c$ , and reservoir volume trade off against each other if the time constant is known. Reasonable limits for these parameters are given in the supporting information.

The viscosity, compressibility, conduit length and reservoir volume are all linearly proportional to the time constant, such that an increase in one parameter could be offset by an equivalent decrease by another (Figs. 8e and f). The conduit length is constrained to  $8 \pm 2$  km by petrological estimates of the depth of the reservoir top and therefore uncertainties on  $L_c$  are approximately 25 % [Ridolfi et al., 2008; Samaniego et al., 2008], however the other three parameters are all be subject to order of magnitude uncertainties.

Figure 8d shows the strong dependence of  $t_c$  on conduit dimensions and conduit cross-section aspect ratio  $r_A$ , which is 1 if the conduit is a cylindrical pipe and larger for dyke-like geometries. Taking the 24 m diameter spine on 28 September 2014 as an indication of the uppermost conduit dimensions gives a conduit with a cross-sectional area of  $450 \text{ m}^2$ . Using this area for the entire length of the conduit gives a strongly elliptical conduit with  $a = 85$  m and  $b = 1.7$  m and an aspect ratio of  $\sim 50$  (filled circles in Fig. 8d). However, given the uncertainties in  $V_0$ ,  $\bar{\eta}$ , and  $\bar{\beta}$ , other conduit aspect ratios and geometries are possible.





723 **Figure 8.** a) Schematic representation of the magma reservoir used in the models, including the source  
 724 region for the deformation signal discussed in Section 4. b) Relative fit of different models with constant  
 725 recharge rates to the lava extrusion observations. c) Misfit plot, showing the root mean square error (RMSE)  
 726 of models with different constant recharge rate (solid black line) and the trade-off between recharge rate and  
 727 time constant (dot-dashed black line). In all plots the solid red lines indicate the observed time constant ( $\sim$   
 728 2000 days) assuming there is no magma recharge ( $q_{in} = 0$ ), and the dashed blue lines give the best fitting  
 729 time constant ( $\sim 170$  days) assuming magma recharge at a constant rate ( $q_{in} = 0.29 \text{ m}^3\text{s}^{-1}$ ). d)–f) Plots of  $t_c$   
 730 dependence on reservoir parameters: d) conduit cross section dimensions and aspect ratio, e) compressibility  
 731 and magma viscosity, f) conduit length and reservoir volume. In each plot, all other parameters are kept con-  
 732 stant at the given values. In f), the solid lines are plotted using the parameters given for a closed system, while  
 733 the dotted lines are using the given open system parameters. The filled circles in d) give the value of  $b$  and  $t_c$   
 734 at given aspect ratios assuming the conduit cross sectional area is equal to that of the lava spine observed on  
 735 28 September 2014.

### 5.2.2 Temporal evolution of an open system

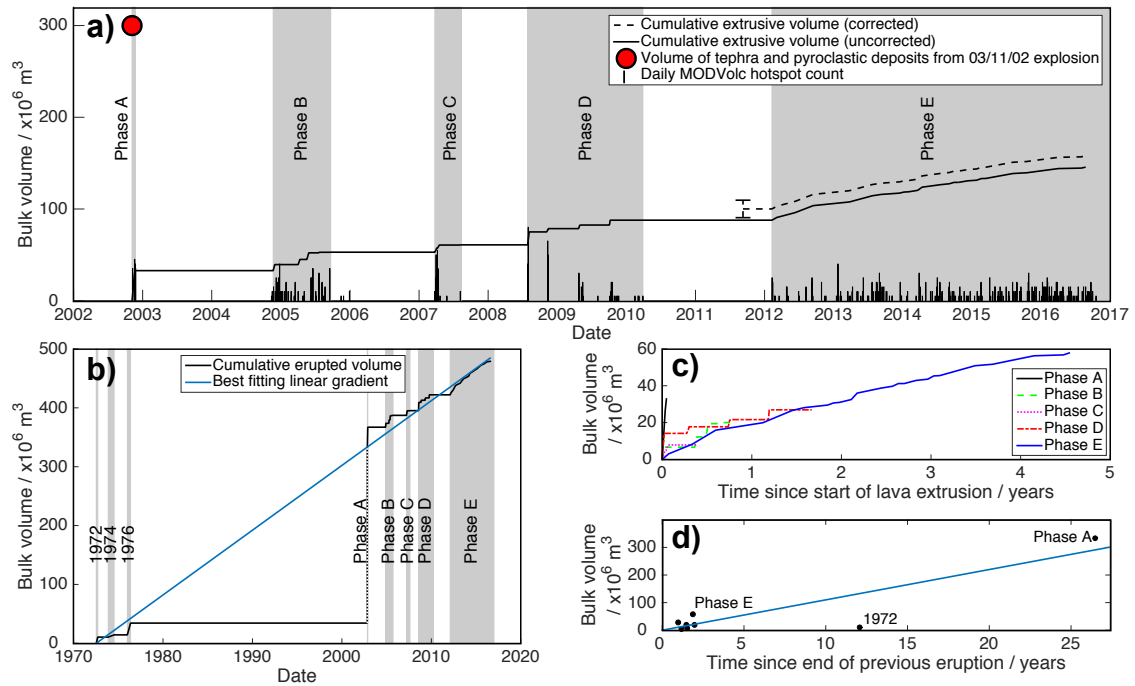
If we instead consider the magmatic reservoir at El Reventador to be supplied with melt from below at a constant rate ( $q_{in} > 0$ ), we can also model a good fit to the data (blue dashed line in Fig. 6a), with  $t_c = 170$  days and 95 % confidence limits between 110 and 350 days. The time-averaged extrusion rate decreased gradually over the first year of lava extrusion and reached an effectively constant gradient by mid 2013. From equation 9 this linear gradient is equivalent to the constant influx rate, which gives  $q_{in} = 0.36 \pm 0.01 \text{ m}^3\text{s}^{-1}$  for Phase E at El Reventador. Assuming the lava flows have a vesicularity of 20 % gives a influx rate of  $0.29 \pm 0.01 \text{ m}^3\text{s}^{-1}$  DRE.

The value of  $t_c$  we estimate for this open system model is approximately one order of magnitude lower than if there was no recharge. If we keep all other reservoir parameters the same as for the closed system, then it is impossible to fit the lower time constant given our limits on  $L_c$  and  $V_0$  (Fig. 8f). In order to fit the lower modelled time constant (blue dashed lines in Fig. 8) the magmatic system at El Reventador would require either an order of magnitude lower compressibility or viscosity, or a more cylindrical conduit aspect ratio of  $\sim 4$ . A combination of these factors is likely (dotted lines in Fig. 8f), which would give a value of  $\bar{\beta}$  between  $10^{-10} \text{ Pa}^{-1}$  and  $10^{-9} \text{ Pa}^{-1}$ ,  $\bar{\eta}$  between  $10^5 \text{ Pa s}$  and  $10^6 \text{ Pa s}$ , and a conduit cross section aspect ratio between 4 and 50, with a dyke width between 3.5 m and 12 m respectively.

## 6 Long-term evolution and magma supply rate

The time-averaged discharge rate at El Reventador between 2012 and 2016 shows a gradual decrease on the time scale of months to years. The average bulk eruption rate for the whole 4 year period is  $0.39 \pm 0.03 \text{ m}^3\text{s}^{-1}$ , which gives a DRE rate of  $0.31 \pm 0.02 \text{ m}^3\text{s}^{-1}$ , within error bounds of the average eruption rate between 2002 and 2009 of  $0.33 \pm 0.14 \text{ m}^3\text{s}^{-1}$  [Naranjo *et al.*, 2016]. These eruption rates at El Reventador are similar to the long-term average of 0.3–0.4  $\text{m}^3\text{s}^{-1}$  measured at other long-lived andesitic dome forming eruptions such as Santiaguito, Arenal and Shiveluch [Supplementary Table S1; Harris *et al.*, 2003; Wadge *et al.*, 2006a; Sheldrake *et al.*, 2016]. Here, we place these observations within the context of the earlier phases of eruptive activity at El Reventador.

Naranjo *et al.* [2016] observed 4 distinct phases of activity at El Reventador between 2002 and 2009 (Fig. 9a). The time-averaged discharge rate for Phase A was sig-



765 **Figure 9.** a) Cumulative bulk volume of extruded lava flows at El Reventador since November 2002. The  
 766 solid line plots the cumulative lava volume for Phases A to D from *Naranjo et al.* [2016], with Radarsat-2  
 767 derived volumes for Phase E (Supplementary Table S4). The dashed line shows the cumulative volume dur-  
 768 ing Phase E, starting from the volume measured by the first TanDEM-X acquisition on 9 September 2011,  
 769 plotted with one standard deviation error bars. Vertical black bars show the number of daily hotspot pixels  
 770 detected by the MODVolc algorithm. Grey boxes show phases of lava flow extrusion. The red circle shows  
 771 the estimated volume of magma erupted during the 3 November 2002 paroxysmal phase [*Hall et al.*, 2004].  
 772 b) Cumulative bulk volume of extruded lava flows at El Reventador since November 1972. Volume data for  
 773 1972, 1974, and 1976 are from *Hall et al.* [2004], Phases A to D from *Naranjo et al.* [2016], and Phase E  
 774 from Radarsat-2 amplitude imagery (Supplementary Table S4). The dotted line shows the estimated bulk vol-  
 775 ume erupted in the 3 November 2002 paroxysmal phase [*Hall et al.*, 2004]. The solid blue line shows the best  
 776 fitting linear gradient to the data, which has a gradient of  $0.35 \text{ m}^3 \text{ s}^{-1}$ . c) Cumulative volume of extruded lava  
 777 flows for the five phases of lava extrusion at El Reventador since November 2002. d) Bulk volume erupted  
 778 during each phase against the time interval of quiescence preceding that phase. The blue line has the same  
 779 gradient as the best fit solution to b).

801

**Table 1.** Parameters for best fitting curves to cumulative volume against time at El Reventador.

Phase	Type of fit	$A / \times 10^6$	$B$	$C$	RMSE / $\times 10^6 \text{ m}^3$
B	exponential	23	0.0076		3.1
B	exp + linear	8.9	0.12	0.47	2.1
B	power	1.9	0.42		2.4
D	exponential	25	0.010		4.7
D	exp + linear	14	0.21	0.30	1.7
D	power	4.8	0.27		3.1
E	exponential	98	0.00049		0.34
E	exp + linear	63	0.0060	0.36	0.29
E	power	0.15	0.80		0.25

Exponential curves are of the form  $V = A(1 - e^{-Bt})$ , where  $A$  has units of  $\text{m}^3$ ,  $B$  has units of  $\text{days}^{-1}$ , and  $1/B \equiv t_c$ . Exp + linear curves have the same form as the exponential curve, but with an additional linear term  $+Ct$  where  $C$  has units of  $\text{m}^3\text{day}^{-1}$  and represents a constant rate of magma reservoir recharge. Power law curves are of the form  $V = At^B$ , where  $B$  is dimensionless and  $A$  has units of  $\text{m}^3\text{days}^{-B}$ . In all three equations  $V$  is the cumulative extruded lava volume in  $\text{m}^3$  and  $t$  is the time since the start of the phase in days.

782

nificantly higher than the subsequent phases, which all had rates similar to the start of phase E (Fig. 9c). Phases B and D of lava extrusion appear to have a decrease in extrusion rate throughout the phase and, like Phase E, can be fit by exponential curves of the form  $V = A(1 - e^{-Bt})$  or  $V = A(1 - e^{-Bt}) + Ct$  (Fig. 9c; equation 9), consistent with the behaviour of a depressurising reservoir without and with magma recharge respectively. Phases A and C are shorter in duration than the other phases, and there are not enough data to constrain a best fit curve. The curve for Phase E is less “stepped” in nature than the previous phases due to temporal aliasing of the satellite observations (Fig. 9c). We are unable to determine exactly when a lava flow is emplaced between two satellite image acquisitions, therefore we assume a linear rate of lava extrusion between the first and second image.

793

The data for Phase B, Phase D and Phase E (2012–2016) are all better fit by exponential curves with a constant recharge rate than for no recharge, suggesting the resupply from either the mantle or a deeper reservoir is important at El Reventador (Table 1). From Table 1, and assuming a vesicularity of 20 % for all lavas, the best fitting linear DRE resupply rate was  $0.38 \pm 0.29 \text{ m}^3\text{s}^{-1}$  for Phase B,  $0.24 \pm 0.06 \text{ m}^3\text{s}^{-1}$  for Phase D and  $0.29 \pm 0.01 \text{ m}^3\text{s}^{-1}$  for Phase E. These recharge rates are all broadly similar given error ranges on the earlier phases, consistent with a constant supply rate of melt from below, although as with Phase E, we cannot distinguish between closed and open system models.

802

The extrusion rates for Phase B, Phase D and Phase E can also be fit by a power law curve of the form  $V = At^B$ . For all three phases, the power law curve better fits

803

804 the higher initial extrusion rate at the start of the eruptive phase than the best fitting no-  
 805 recharge exponential solution. Phase B and Phase D are still better fit by an exponential  
 806 with recharge than a power law, however the power law solution to Phase E has a lower  
 807 misfit than either of the exponential solutions, and would plot between the blue and red  
 808 lines on Fig. 6a.

809 While it is currently difficult to significantly distinguish between the three models,  
 810 observations of future lava extrusion should allow better differentiation. As the eruption  
 811 progresses, an exponentially decaying eruption will decrease extrusion rate more signif-  
 812 icantly than one following a power law, which would similarly decrease extrusion rate  
 813 relative to the constant extrusive flux of an effectively open reservoir that is resupplied  
 814 from deep. The power-law equation could therefore be more representative of a magma  
 815 reservoir which is exhibiting behaviour between the end-member cases of a closed system  
 816 without resupply, and that of an open system with constant recharge. Such a system may  
 817 be governed by non-linear resupply rates, in which recharge from below is governed by  
 818 the reservoir pressure [e.g. *Anderson and Segall, 2011; Segall, 2013*].

819 We use volume data from *Hall et al. [2004]* for the previous eruption of El Reven-  
 820 tador during the 1970s in combination with data from *Naranjo et al. [2016]* and our re-  
 821 sults from 2011–2016 to estimate the average extrusion rate over the past four decades  
 822 (Fig. 9b). We find a best fitting linear gradient to the bulk lava volume of  $0.35 \text{ m}^3\text{s}^{-1}$ ,  
 823 with a 95 % confidence interval of  $0.33\text{--}0.38 \text{ m}^3\text{s}^{-1}$ . This rate almost exactly matches the  
 824 linear magma accumulation rate required to match the bulk volume erupted on 3 Novem-  
 825 ber 2002, assuming accumulation started after then end of the previous eruption in 1976.  
 826 Assuming 20 % vesicularity of erupted products would give a decadal DRE rate of  $0.28$   
 827  $\pm 0.02 \text{ m}^3\text{s}^{-1}$ , however the majority of the bulk erupted volume in the paroxysmal phase  
 828 were tephra deposits, which are generally lower density than lava flow deposits [e.g. *Sparks*  
 829 *et al., 1998; Wadge et al., 2010*], therefore  $0.28 \text{ m}^3\text{s}^{-1}$  may be an upper bound on the long  
 830 term DRE extrusion rate. This long-term decadal extrusion rate is almost identical to the  
 831 the time-averaged rate of  $0.27 \pm 0.07 \text{ m}^3\text{s}^{-1}$  DRE for lava flow extrusion postdating the 3  
 832 November 2002 explosion and also agrees well with the  $0.29 \pm 0.01 \text{ m}^3\text{s}^{-1}$  linear magma  
 833 supply rate derived from Phase E.

834 Since the range of estimated linear resupply rates between  $0.2$  and  $0.4 \text{ m}^3\text{s}^{-1}$  matches  
 835 well with the long term DRE eruption rate at El Reventador, we infer that there has been

no significant long term increase in the volume of magma stored underneath El Reventador since 2002, implying a low likelihood of an eruption of similar magnitude to the November 2002 event. However, Fig. 9d shows that the volume extruded in the 1972 eruption was much lower than expected given the pre-eruption repose period of 12 years. The approximately constant magma supply observed over the past four decades therefore appears to be different to the pre-1972 supply rate.

## 7 Conclusions

We use satellite radar data to measure the volume of extruded lava at El Reventador volcano, Ecuador between 2011 and 2016. We find a total DRE lava volume of  $44.8\text{M} \pm 2.5\text{M} \text{ m}^3$  was erupted between 9 February 2012 and 24 August 2016 at an average rate of  $0.31 \pm 0.02 \text{ m}^3\text{s}^{-1}$ , during a phase of lava extrusion that is still ongoing at the time of writing. This period of extrusion exhibited much more continuous activity than previous, shorter duration, eruptive phases at El Reventador. The average lava extrusion rate between February 2012 and August 2016 decreased gradually and can be equally well fit by models equivalent to a depressurising reservoir without magma recharge, or a reservoir that is being supplied with melt from below at a constant rate, which has an upper bound of  $0.35 \pm 0.01 \text{ m}^3\text{s}^{-1}$ .

We observe one period of ground deformation between 9 March and 10 June 2012, in which the pattern of ground deformation suggests a small, shallow, vertical, north-south oriented dyke opening underneath the summit. There are no other magmatic deformation events visible in interferograms covering 2012–2016, suggesting that the magma source is likely deep, large, highly compressible, or being resupplied from the lower crust or mantle. While there are large trade offs between the reservoir volume and compressibility, we show that the reservoir is larger than  $3 \text{ km}^3$  and the eruption is supplied through a conduit that is a dyke extending to a depth of 8 km. This dyke has a cross section aspect ratio between 4 and 50, or lateral dimension between 12 m by 48 m and 3.5 m by 170 m.

We show the benefit of using radar amplitude imagery to supplement InSAR phase measurements of topographic change at erupting volcanoes. Such measurements could be usefully applied to other volcanic settings where radar phase measurements decorrelate, for instance due to infrequent SAR acquisitions, resurfacing by volcanic activity or vegetation growth.

## Acknowledgments

We thank M. Bagnardi, K. Cashman, M.E. Pritchard and P. Segall for useful discussions and comments. DA is supported by a NERC studentship. JB, GW, and SKE are supported by NERC COMET. JB and SKE are supported by STREVA, and SKE is supported by the Leverhulme Trust. The data used are listed in the supporting information. Satellite data were provided through the Committee of Earth Observation Satellites (CEOS) Volcano Pilot for Disaster Risk Reduction. Radarsat-2 data were provided by the Canadian Space Agency and MacDonald Dettwiler & Associates Ltd. through proposal SOAR-geohazards-5297. TanDEM-X data were provided by Deutsches Zentrum für Luft- und Raumfahrt e. V. (DLR; German Space Agency) through proposal NTI\_BIST7067.

## References

- Albino, F., B. Smets, N. D'Oreye, and F. Kervyn (2015), High-resolution TanDEM-X DEM: An accurate method to estimate lava flow volumes at Nyamulagira Volcano (D. R. Congo), *J. Geophys. Res. Solid Earth*, *120*(6), 4189–4207, doi: 10.1002/2015JB011988.
- Amoruso, A., and L. Crescentini (2009), Shape and volume change of pressurized ellipsoidal cavities from deformation and seismic data, *J. Geophys. Res. Solid Earth*, *114*(2), B02,210, doi:10.1029/2008JB005946.
- Anderson, K., and P. Segall (2011), Physics-based models of ground deformation and extrusion rate at effusively erupting volcanoes, *J. Geophys. Res.*, *116*(B7), B07,204, doi: 10.1029/2010JB007939.
- Anderson, K., and P. Segall (2013), Bayesian inversion of data from effusive volcanic eruptions using physics-based models: Application to Mount St. Helens 2004-2008, *J. Geophys. Res. Solid Earth*, *118*(5), 2017–2037, doi:10.1002/jgrb.50169.
- Anderson, K., and P. Segall (2014), Magma Reservoir Volumes and Eruption Forecasting. Oral presentation at *Euro. Geosci. Union Gen. Assem.*, Vienna, 27 April–2 May, 2014, abstract id.15256
- Anderson, K., M. Lisowski, and P. Segall (2010), Cyclic ground tilt associated with the 2004-2008 eruption of Mount St. Helens, *J. Geophys. Res. Solid Earth*, *115*(11), doi: 10.1029/2009JB007102.

- 897 Anderson, K. R., and M. P. Poland (2016), Bayesian estimation of magma supply, storage,  
898 and eruption rates using a multiphysical volcano model: Kīlauea Volcano, 2000-2012,  
899 *Earth Planet. Sci. Lett.*, *447*, 161–171, doi:10.1016/j.epsl.2016.04.029.
- 900 Arnold, D. W. D., J. Biggs, G. Wadge, S. K. Ebmeier, H. M. Odbert, and M. P. Poland  
901 (2016), Dome growth, collapse, and valley fill at Soufrière Hills Volcano, Montserrat,  
902 from 1995 to 2013: Contributions from satellite radar measurements of topographic  
903 change, *Geosphere*, *12*(4), 1300–1315, doi:10.1130/GES01291.1.
- 904 Aspinall, W., H. Sigurdsson, and J. Shepherd (1973), Eruption of Soufrière Vol-  
905 cano on St. Vincent Island, 1971-1972, *Science* (80-. ), *181*(4095), 117–124, doi:  
906 10.1126/science.181.4095.117.
- 907 Bagnardi, M., P. J. González, and A. Hooper (2016), High-resolution digital elevation  
908 model from tri-stereo Pleiades-1 satellite imagery for lava flow volume estimates at  
909 Fogo Volcano, *Geophys. Res. Lett.*, *43*(12), 6267–6275, doi:10.1002/2016GL069457.
- 910 Belousov, A., B. Voight, M. Belousova, and A. Petukhin (2002), Pyroclastic surges and  
911 flows from the 8-10 May 1997 explosive eruption of Bezymianny volcano, Kamchatka,  
912 Russia, *Bull. Volcanol.*, *64*(7), 455–471, doi:10.1007/s00445-002-0222-5.
- 913 Biggs, J., S. K. Ebmeier, W. P. Aspinall, Z. Lu, M. E. Pritchard, R. S. J. Sparks, and T. A.  
914 Mather (2014), Global link between deformation and volcanic eruption quantified by  
915 satellite imagery., *Nat. Commun.*, *5*, 3471, doi:10.1038/ncomms4471.
- 916 Cashman, K. V., and R. S. J. Sparks (2013), How volcanoes work: A 25 year perspective,  
917 *Geol. Soc. Am. Bull.*, *125*(5-6), 664–690, doi:10.1130/B30720.1.
- 918 Cashman, K. V., S. A. Soule, B. H. Mackey, N. I. Deligne, N. D. Deardorff, and H. R.  
919 Dietterich (2013), How lava flows: New insights from applications of lidar technologies  
920 to lava flow studies, *Geosphere*, *9*(6), 1664–1680, doi:10.1130/GES00706.1.
- 921 Chaussard, E., F. Amelung, and Y. Aoki (2013), Characterization of open and closed vol-  
922 canic systems in Indonesia and Mexico using InSAR time series, *J. Geophys. Res. Solid*  
923 *Earth*, *118*(8), 3957–3969, doi:10.1002/jgrb.50288.
- 924 Cigolini, C., A. Borgia, and L. Casertano (1984), Intra-crater activity, a’-a-block lava, vis-  
925 cosity and flow dynamics: Arenal Volcano, Costa Rica, *J. Volcanol. Geotherm. Res.*,  
926 *20*(1-2), 155–176, doi:10.1016/0377-0273(84)90072-6.
- 927 Coombs, M. L., K. F. Bull, J. W. Vallance, D. J. Schneider, E. E. Thoms, R. L. Wessels,  
928 and R. G. McGimsey (2010), Timing, distribution and volume of proximal products of  
929 the 2006 eruption of Augustine Volcano, *2006 Erupt. Augustine Volcano, Alaska*, pp.



- 930 145–185.
- 931 Costa, A., O. Melnik, R. S. J. Sparks, and B. Voight (2007), Control of magma flow  
932 in dykes on cyclic lava dome extrusion, *Geophys. Res. Lett.*, *34*(2), L02,303, doi:  
933 10.1029/2006GL027466.
- 934 Dearnorff, N. D., and K. V. Cashman (2012), Emplacement conditions of the c. 1,600-year  
935 bp Collier Cone lava flow, Oregon: a LiDAR investigation, *Bull. Volcanol.*, *74*(9), 2051–  
936 2066, doi:10.1007/s00445-012-0650-9.
- 937 Denlinger, R. P. (1997), A dynamic balance between magma supply and eruption rate at  
938 Kilauea volcano, Hawaii, *J. Geophys. Res.*, *102*(B8), 18,091, doi:10.1029/97JB01071.
- 939 Diefenbach, A. K., K. F. Bull, R. L. Wessels, and R. G. McGimsey (2013), Photogram-  
940 metric monitoring of lava dome growth during the 2009 eruption of Redoubt Volcano,  
941 *J. Volcanol. Geotherm. Res.*, *259*, 308–316, doi:10.1016/j.jvolgeores.2011.12.009.
- 942 Dieterich, J. H., and R. W. Decker (1975), Finite element modeling of surface de-  
943 formation associated with volcanism, *J. Geophys. Res.*, *80*(29), 4094–4102, doi:  
944 10.1029/JB080i029p04094.
- 945 Dietterich, H. R., M. P. Poland, D. A. Schmidt, K. V. Cashman, D. R. Sherrod, and A. T.  
946 Espinosa (2012), Tracking lava flow emplacement on the east rift zone of Kilauea,  
947 Hawai'i, with synthetic aperture radar coherence, *Geochemistry Geophys. Geosystems*,  
948 *13*, Q05,001, doi:10.1029/2011GC004016.
- 949 Dvorak, J. J., and D. Dzurisin (1993), Variations in magma supply rate at Kilauea Vol-  
950 cano, Hawai'i, *J. Geophys. Res.*, *98*(B12), 22,255, doi:10.1029/93JB02765.
- 951 Dvorak, J. J., and A. T. Okamura (1987), A hydraulic model to explain variations in sum-  
952 mit tilt rate at Kilauea and Mauna Loa Volcanoes, *US Geol. Surv. Prof. Pap. 1350*, pp.  
953 1281 – 1296.
- 954 Dzurisin, D. (2003), A comprehensive approach to monitoring volcano deformation as a  
955 window on the eruption cycle, *Rev. Geophys.*, *41*(2), 1–29, doi:10.1029/2003RG000134.
- 956 Dzurisin, D. (2007), *Volcano deformation : geodetic monitoring techniques*, xxxv, 441 p.  
957 pp., Springer-Praxis, Chichester, UK, doi:10.1007/978-3-540-49302-0.
- 958 Ebmeier, S., J. Biggs, T. Mather, J. Elliott, G. Wadge, and F. Amelung (2012), Measuring  
959 large topographic change with InSAR: Lava thicknesses, extrusion rate and subsidence  
960 rate at Santiaguito volcano, Guatemala, *Earth Planet. Sci. Lett.*, *335-336*, 216–225, doi:  
961 10.1016/j.epsl.2012.04.027.

- 962 Ebmeier, S. K., J. Biggs, T. A. Mather, and F. Amelung (2013a), Applicability of InSAR  
 963 to tropical volcanoes: insights from Central America, *Geol. Soc. London, Spec. Publ.*,  
 964 380(1), 15–37, doi:10.1144/SP380.2.
- 965 Ebmeier, S. K., J. Biggs, T. A. Mather, and F. Amelung (2013b), On the lack of InSAR  
 966 observations of magmatic deformation at Central American volcanoes, *J. Geophys. Res.*  
 967 *Solid Earth*, 118(5), 2571–2585, doi:10.1002/jgrb.50195.
- 968 Ebmeier, S. K., J. Biggs, C. Muller, and G. Avard (2014), Thin-skinned mass-wasting re-  
 969 sponsible for widespread deformation at Arenal volcano, *Front. Earth Sci.*, 2(December),  
 970 1–10, doi:10.3389/feart.2014.00035.
- 971 Fink, J. H., and R. W. Griffiths (1998), Morphology, eruption rates, and rheology of  
 972 lava domes: Insights from laboratory models, *J. Geophys. Res.*, 103(B1), 527, doi:  
 973 10.1029/97JB02838.
- 974 Fournier, T. J., M. E. Pritchard, and S. N. Riddick (2010), Duration, magnitude, and fre-  
 975 quency of subaerial volcano deformation events: New results from Latin America us-  
 976 ing InSAR and a global synthesis, *Geochemistry, Geophys. Geosystems*, 11(1), doi:  
 977 10.1029/2009GC002558.
- 978 Global Volcanism Program (2012), Report on Reventador (Ecuador), *Tech. Rep. 3*, Smith-  
 979 sonian Institution, doi:10.5479/si.GVP.BGVN201203-352010.
- 980 Goldstein, R. M., and C. L. Werner (1998), Radar interferogram filtering for geophysical  
 981 applications, *Geophys. Res. Lett.*, 25(21), 4035–4038, doi:10.1029/1998GL900033.
- 982 González, P. J., M. Bagnardi, A. J. Hooper, Y. Larsen, P. Marinkovic, S. V. Samsonov,  
 983 and T. J. Wright (2015), The 2014–2015 eruption of Fogo volcano: Geodetic model-  
 984 ing of Sentinel-1 TOPS interferometry, *Geophys. Res. Lett.*, 42(21), 9239–9246, doi:  
 985 10.1002/2015GL066003.
- 986 Gottsmann, J., A. Folch, and H. Rymer (2006), Unrest at Campi Flegrei: A contribution to  
 987 the magmatic versus hydrothermal debate from inverse and finite element modeling, *J.*  
 988 *Geophys. Res.*, 111(B7), B07,203, doi:10.1029/2005JB003745.
- 989 Gudmundsson, M. T., K. Jónsdóttir, A. Hooper, E. P. Holohan, S. A. Halldórsson, B. G.  
 990 Ófeigsson, S. Cesca, K. S. Vogfjörð, F. Sigmundsson, T. Högnadóttir, P. Einarsson,  
 991 O. Sigmarrsson, A. H. Jarosch, K. Jónasson, E. Magnússon, S. Hreinsdóttir, M. Bag-  
 992 nardi, M. M. Parks, V. Hjörleifsdóttir, F. Pálsson, T. R. Walter, M. P. J. Schöpfer,  
 993 S. Heimann, H. I. Reynolds, S. Dumont, E. Bali, G. H. Gudfinnsson, T. Dahm, M. J.  
 994 Roberts, M. Hensch, J. M. C. Belart, K. Spaans, S. Jakobsson, G. B. Gudmunds-

- 995 son, H. M. Fridriksdóttir, V. Drouin, T. Dürig, G. Aðalgeirsdóttir, M. S. Riishuus,  
 996 G. B. M. Pedersen, T. van Boeckel, B. Oddsson, M. A. Pfeffer, S. Barsotti, B. Bergs-  
 997 son, A. Donovan, M. R. Burton, and A. Aiuppa (2016), Gradual caldera collapse at  
 998 Bárðarbunga volcano, Iceland, regulated by lateral magma outflow, *Science* (80-. ),  
 999 353(6296), 1–24, doi:10.1126/science.aaf8988.sciencemag.org.
- 1000 Gudmundsson, A. (2016), The mechanics of large volcanic eruptions, doi:  
 1001 10.1016/j.earscirev.2016.10.003.
- 1002 Hall, M., P. Ramón, P. Mothes, J. L. LePennec, A. García, P. Samaniego, and H. Yepes  
 1003 (2004), Volcanic eruptions with little warning: the case of Volcán Reventador’s Sur-  
 1004 prise November 3, 2002 Eruption, Ecuador, *Rev. geológica Chile*, 31(2), 349–358, doi:  
 1005 10.4067/S0716-02082004000200010.
- 1006 Harris, A. J. L., J. B. Murray, S. E. Aries, M. A. Davies, L. P. Flynn, M. J. Wooster,  
 1007 R. Wright, and D. A. Rothery (2000), Effusion rate trends at Etna and Krafla and their  
 1008 implications for eruptive mechanisms, *J. Volcanol. Geotherm. Res.*, 102(3-4), 237–270,  
 1009 doi:10.1016/S0377-0273(00)00190-6.
- 1010 Harris, A. J., W. I. Rose, and L. P. Flynn (2003), Temporal trends in lava dome extru-  
 1011 sion at Santiaguito 1922–2000, *Bull. Volcanol.*, 65(2-3), 77–89, doi:10.1007/s00445-002-  
 1012 0243-0.
- 1013 Harris, A. J. L., J. Dehn, and S. Calvari (2007), Lava effusion rate definition and measure-  
 1014 ment: a review, *Bull. Volcanol.*, 70(1), 1–22, doi:10.1007/s00445-007-0120-y.
- 1015 Hautmann, S., D. Hidayat, N. Fournier, A. T. Linde, I. S. Sacks, and C. P. Williams  
 1016 (2013), Pressure changes in the magmatic system during the December 2008/Jan-  
 1017 uary 2009 extrusion event at Soufrière Hills Volcano, Montserrat (W.I.), de-  
 1018 rived from strain data analysis, *J. Volcanol. Geotherm. Res.*, 250, 34–41, doi:  
 1019 10.1016/j.jvolgeores.2012.10.006.
- 1020 Hickey, J., and J. Gottsmann (2014), Benchmarking and developing numerical Finite Ele-  
 1021 ment models of volcanic deformation, *J. Volcanol. Geotherm. Res.*, 280, 126–130, doi:  
 1022 10.1016/j.jvolgeores.2014.05.011.
- 1023 Hooper, A., J. Pietrzak, W. Simons, H. Cui, R. Riva, M. Naeije, A. Terwisscha van  
 1024 Scheltinga, E. Schrama, G. Stelling, and A. Socquet (2013), Importance of horizontal  
 1025 seafloor motion on tsunami height for the 2011 Mw=9.0 Tohoku-Oki earthquake, doi:  
 1026 10.1016/j.epsl.2012.11.013.

- 1027 Hreinsdóttir, S., F. Sigmundsson, M. J. Roberts, H. Björnsson, R. Grapenthin, P. Arason,  
 1028 T. Árnadóttir, J. Hólmjárn, H. Geirsson, R. a. Bennett, M. T. Gudmundsson, B. Odds-  
 1029 son, B. G. Ófeigsson, T. Villemin, T. Jónsson, E. Sturkell, Á. Höskuldsson, G. Larsen,  
 1030 T. Thordarson, and B. A. Óladóttir (2014), Volcanic plume height correlated with  
 1031 magma-pressure change at Grímsvötn Volcano, Iceland, *Nat. Geosci.*, *7*(3), 214–218,  
 1032 doi:10.1038/ngeo2044.
- 1033 Huppert, H. E., J. B. Shepherd, R. Haraldur Sigurdsson, and S. J. Sparks (1982), On lava  
 1034 dome growth, with application to the 1979 lava extrusion of the Soufrière of St. Vin-  
 1035 cent, *J. Volcanol. Geotherm. Res.*, *14*(3-4), 199–222, doi:10.1016/0377-0273(82)90062-2.
- 1036 Huppert, H. E., and A. W. Woods (2002), The role of volatiles in magma chamber dynam-  
 1037 ics., *Nature*, *420*(6915), 493–495, doi:10.1038/nature01211.
- 1038 Johnson, J. B., J. M. Lees, A. Gerst, D. Sahagian, and N. Varley (2008), Long-period  
 1039 earthquakes and co-eruptive dome inflation seen with particle image velocimetry., *Na-  
 1040 ture*, *456*(7220), 377–381, doi:10.1038/nature07429.
- 1041 Jones, L. K., P. R. Kyle, C. Oppenheimer, J. D. Frechette, and M. H. Okal (2015), Ter-  
 1042 restrial laser scanning observations of geomorphic changes and varying lava lake  
 1043 levels at Erebus volcano, Antarctica, *J. Volcanol. Geotherm. Res.*, *295*, 43–54, doi:  
 1044 10.1016/j.jvolgeores.2015.02.011.
- 1045 Kelfoun, K., and S. Vallejo Vargas (2015), VolcFlow capabilities and potential develop-  
 1046 ment for the simulation of lava flows, *Geol. Soc. London, Spec. Publ.*, *426*(1), SP426.8–,  
 1047 doi:10.1144/SP426.8.
- 1048 Kozono, T., H. Ueda, T. Ozawa, T. Koyaguchi, E. Fujita, A. Tomiya, and Y. J. Suzuki  
 1049 (2013), Magma discharge variations during the 2011 eruptions of Shinmoe-dake vol-  
 1050 cano, Japan, revealed by geodetic and satellite observations, *Bull. Volcanol.*, *75*(3), 1–  
 1051 13, doi:10.1007/s00445-013-0695-4.
- 1052 Kubanek, J., M. Westerhaus, A. Schenk, N. Aisyah, K. S. Brotopuspito, and B. Heck  
 1053 (2015), Volumetric change quantification of the 2010 Merapi eruption using TanDEM-X  
 1054 InSAR, *Remote Sens. Environ.*, *164*, 16–25, doi:10.1016/j.rse.2015.02.027.
- 1055 Lekner, J. (2007), Viscous flow through pipes of various cross-sections, *J. Phys.*, *28*(3),  
 1056 521–527, doi:10.1088/0143-0807/28/3/014.
- 1057 Leshner, C. E., and F. J. Spera (2015), *Thermodynamic and Transport Properties of Silicate  
 1058 Melts and Magma*, 113–141 pp., Elsevier, doi:10.1016/B978-0-12-385938-9.00005-5.

- 1059 Lu, Z., T. Masterlark, D. Dzurisin, R. Rykhus, and C. Wicks (2003), Magma supply dy-  
1060 namics at Westdahl volcano, Alaska, modeled from satellite radar interferometry, *J.*  
1061 *Geophys. Res. Earth*, *108*(B7), 2354, doi:10.1029/2002JB002311.
- 1062 Massonnet, D., and K. L. Feigl (1998), Radar interferometry and its application to  
1063 changes in the Earth's surface, *Rev. Geophys.*, *36*(4), 441, doi:10.1029/97RG03139.
- 1064 Mastin, L., E. Roeloffs, and N. Beeler (2008), Constraints on the size, overpressure, and  
1065 volatile content of the Mount St. Helens magma system from geodetic and dome-  
1066 growth measurements during the 2004–2006+ eruption, *A Volcano Rekindled: the re-*  
1067 *newed eruption of Mount St. Helens, 2004–2006*, U.S. Geol. Surv. ch. 22, 461-488 pp.  
1068 <http://pubs.er.usgs.gov/publication/pp175022>
- 1069 Mastin, L. G., M. Lisowski, E. Roeloffs, and N. Beeler (2009), Improved constraints on  
1070 the estimated size and volatile content of the Mount St. Helens magma system from  
1071 the 2004–2008 history of dome growth and deformation, *Geophys. Res. Lett.*, *36*(20),  
1072 L20,304, doi:10.1029/2009GL039863.
- 1073 McCormick-Kilbride, B., M. Edmonds, and J. Biggs (2016), Observing eruptions  
1074 of gas-rich compressible magmas from space., *Nat. Commun.*, *7*, 13,744, doi:  
1075 10.1038/ncomms13744.
- 1076 McTigue, D. F. (1987), Elastic stress and deformation near a finite spherical magma body:  
1077 Resolution of the point source paradox, *J. Geophys. Res.*, *92*(B12), 12,931–12,940, doi:  
1078 10.1029/JB092iB12p12931.
- 1079 Melnik, O., and R. S. J. Sparks (2005), Controls on conduit magma flow dynamics dur-  
1080 ing lava dome building eruptions, *J. Geophys. Res. B Solid Earth*, *110*(2), 1–21, doi:  
1081 10.1029/2004JB003183.
- 1082 Miller, T. P. (1994), Dome growth and destruction during the 1989-1990 eruption of  
1083 Redoubt volcano, *J. Volcanol. Geotherm. Res.*, *62*(1-4), 197–212, doi:10.1016/0377-  
1084 0273(94)90034-5.
- 1085 Mogi, K. (1958), Relations between the eruptions of various volcanoes and the deforma-  
1086 tions of the ground surfaces around them, doi:10.1016/j.epsl.2004.04.016.
- 1087 Morales Rivera, A. M., F. Amelung, and P. Mothes (2016), Volcano deformation survey  
1088 over the Northern and Central Andes with ALOS InSAR time series, *Geochemistry,*  
1089 *Geophys. Geosystems*, *17*(7), 2869–2883, doi:10.1002/2016GC006393.
- 1090 Moran, S. C., O. Kwoun, T. Masterlark, and Z. Lu (2006), On the absence of InSAR-  
1091 detected volcano deformation spanning the 1995–1996 and 1999 eruptions of

- 1092 Shishaldin Volcano, Alaska, *J. Volcanol. Geotherm. Res.*, 150(1-3), 119–131, doi:  
1093 10.1016/j.jvolgeores.2005.07.013.
- 1094 Mosegaard, K., and A. Tarantola (1995), Monte Carlo sampling of solutions to  
1095 inverse problems, *J. Geophys. Res. Solid Earth*, 100(B7), 12,431–12,447, doi:  
1096 10.1029/94JB03097.
- 1097 Nakada, S., H. Shimizu, and K. Ohta (1999), Overview of the 1990–1995 eruption  
1098 at Unzen Volcano, *J. Volcanol. Geotherm. Res.*, 89(1-4), 1–22, doi:10.1016/S0377-  
1099 0273(98)00118-8.
- 1100 Naranjo, J. A., R. S. J. Sparks, M. V. Stasiuk, H. Moreno, and G. J. Ablay (1992), Mor-  
1101 phological, structural and textural variations in the 1988–1990 andesite lava of Lon-  
1102 quimay volcano, Chile, *Geol. Mag.*, 129(6), 657–678, doi:10.1017/S0016756800008426.
- 1103 Naranjo, M. F. (2013), Estudio petro-geoquímico y cronológico de los flujos de lava emi-  
1104 tidos por el volcán Reventador entre 2002 a 2009, Masters thesis, Escuela Politécnica  
1105 Nacional. <http://bibdigital.epn.edu.ec/handle/15000/6443>
- 1106 Naranjo, M. F., S. K. Ebmeier, S. Vallejo, P. Ramón, P. Mothes, J. Biggs, and F. Herrera  
1107 (2016), Mapping and measuring lava volumes from 2002 to 2009 at El Reventador Vol-  
1108 cano, Ecuador, from field measurements and satellite remote sensing, *J. Appl. Volcanol.*,  
1109 5(1), 8, doi:10.1186/s13617-016-0048-z.
- 1110 Navarro-Ochoa, C., J. C. Gavilanes-Ruíz, and A. Cortés-Cortés (2002), Movement  
1111 and emplacement of lava flows at Volcán de Colima, México: November 1998-  
1112 February 1999, *J. Volcanol. Geotherm. Res.*, 117(1-2), 155–167, doi:10.1016/S0377-  
1113 0273(02)00242-1.
- 1114 Nomikou, P., M. M. Parks, D. Papanikolaou, D. M. Pyle, T. A. Mather, S. Carey, A. B.  
1115 Watts, M. Paulatto, M. L. Kalnins, I. Livanos, K. Bejelou, E. Simou, and I. Perros  
1116 (2014), The emergence and growth of a submarine volcano: The Kameni islands, San-  
1117 torini (Greece), *GeoResJ*, 1-2, 8–18, doi:10.1016/j.grj.2014.02.002.
- 1118 Okada, Y. (1985), Surface deformation due to shear and tensile faults in a half-space,  
1119 *Int. J. Rock Mech. Min. Sci. Geomech. Abstr.*, 75(4), 1135–1154, doi:10.1016/0148-  
1120 9062(86)90674-1.
- 1121 Pallister, J. S., D. J. Schneider, J. P. Griswold, R. H. Keeler, W. C. Burton, C. Noyles,  
1122 C. G. Newhall, and A. Ratdompurbo (2013), Merapi 2010 eruption-Chronology and  
1123 extrusion rates monitored with satellite radar and used in eruption forecasting, *J. Vol-  
1124 canol. Geotherm. Res.*, 261, 144–152, doi:10.1016/j.jvolgeores.2012.07.012.

- 1125 Parker, A. L., J. Biggs, R. J. Walters, S. K. Ebmeier, T. J. Wright, N. A. Teanby,  
 1126 and Z. Lu (2015), Systematic assessment of atmospheric uncertainties for In-  
 1127 SAR data at volcanic arcs using large-scale atmospheric models: Application to  
 1128 the Cascade volcanoes, United States, *Remote Sens. Environ.*, *170*, 102–114, doi:  
 1129 10.1016/j.rse.2015.09.003.
- 1130 Peltier, A., P. Bachèlery, and T. Staudacher (2009), Magma transport and storage at  
 1131 Piton de La Fournaise (La Réunion) between 1972 and 2007: A review of geo-  
 1132 physical and geochemical data, *J. Volcanol. Geotherm. Res.*, *184*(1-2), 93–108, doi:  
 1133 10.1016/j.jvolgeores.2008.12.008.
- 1134 Pinel, V., A. Hooper, S. De la Cruz-Reyna, G. Reyes-Davila, M. Doin, and P. Bascou  
 1135 (2011), The challenging retrieval of the displacement field from InSAR data for an-  
 1136 desitic stratovolcanoes: Case study of Popocatepetl and Colima Volcano, Mexico, *J.*  
 1137 *Volcanol. Geotherm. Res.*, *200*(1-2), 49–61, doi:10.1016/j.jvolgeores.2010.12.002.
- 1138 Pinel, V., M. Poland, and A. Hooper (2014), Volcanology: Lessons learned from  
 1139 Synthetic Aperture Radar imagery, *J. Volcanol. Geotherm. Res.*, *289*, 81–113, doi:  
 1140 10.1016/j.jvolgeores.2014.10.010.
- 1141 Poland, M. P., A. Miklius, A. Jeff Sutton, and C. R. Thornber (2012), A mantle-driven  
 1142 surge in magma supply to Kīlauea Volcano during 2003–2007, *Nat. Geosci.*, *5*(4), 295–  
 1143 300, doi:10.1038/ngeo1426.
- 1144 Poland, M. P. (2014), Time-averaged discharge rate of subaerial lava at Kīlauea Volcano,  
 1145 Hawai'i, measured from TanDEM-X interferometry: Implications for magma supply  
 1146 and storage during 2011–2013, *J. Geophys. Res. Solid Earth*, *119*(7), 5464–5481, doi:  
 1147 10.1002/2014JB011132.
- 1148 Pritchard, M. E., and M. Simons (2002), A satellite geodetic survey of large-scale de-  
 1149 formation of volcanic centres in the central Andes., *Nature*, *418*(6894), 167–71, doi:  
 1150 10.1038/nature00872.
- 1151 Ratdomopurbo, A., F. Beauducel, J. Subandriyo, I. G. M. Agung Nandaka, C. G.  
 1152 Newhall, Suharna, D. S. Sayudi, H. Suparwaka, and Sunarta (2013), Overview of  
 1153 the 2006 eruption of Mt. Merapi, *J. Volcanol. Geotherm. Res.*, *261*, 87–97, doi:  
 1154 10.1016/j.jvolgeores.2013.03.019.
- 1155 Reverso, T., J. Vandemeulebrouck, F. Jouanne, V. Pinel, T. Villemin, E. Sturkell, and  
 1156 P. Bascou (2014), A two-magma chamber model as a source of deformation at  
 1157 Grímsvötn Volcano, Iceland, *J. Geophys. Res. Solid Earth*, *119*(6), 4666–4683, doi:



- 1158 10.1002/2013JB010569.
- 1159 Ridolfi, F., M. Puerini, A. Renzulli, M. Menna, and T. Toulkeridis (2008), The magmatic  
 1160 feeding system of El Reventador volcano (Sub-Andean zone, Ecuador) constrained by  
 1161 texture, mineralogy and thermobarometry of the 2002 erupted products, *J. Volcanol.*  
 1162 *Geotherm. Res.*, 176(1), 94–106, doi:10.1016/j.jvolgeores.2008.03.003.
- 1163 Rivalta, E., and P. Segall (2008), Magma compressibility and the missing source for some  
 1164 dike intrusions, *Geophys. Res. Lett.*, 35(4), L04,306, doi:10.1029/2007GL032521.
- 1165 Rymer, H., and G. Williams-Jones (2000), Volcanic eruption prediction: Magma chamber  
 1166 physics from gravity and deformation measurements, *Geophys. Res. Lett.*, 27(16), 2389–  
 1167 2392, doi:10.1029/1999GL011293.
- 1168 Salzer, J. T., M. Nikkhoo, T. R. Walter, H. Sudhaus, G. Reyes-Dávila, M. Bretón, and  
 1169 R. Arámbula (2014), Satellite radar data reveal short-term pre-explosive displacements  
 1170 and a complex conduit system at Volcán de Colima, Mexico, *Front. Earth Sci.*, 2(June),  
 1171 1–11, doi:10.3389/feart.2014.00012.
- 1172 Samaniego, P., J. P. Eissen, J. L. Le Pennec, C. Robin, M. L. Hall, P. Mothes, D. Chavrit,  
 1173 and J. Cotten (2008), Pre-eruptive physical conditions of El Reventador volcano  
 1174 (Ecuador) inferred from the petrology of the 2002 and 2004–05 eruptions, *J. Volcanol.*  
 1175 *Geotherm. Res.*, 176(1), 82–93, doi:10.1016/j.jvolgeores.2008.03.004.
- 1176 Sanderson, R. W., J. B. Johnson, and J. M. Lees (2010), Ultra-long period seismic sig-  
 1177 nals and cyclic deflation coincident with eruptions at Santiaguito volcano, Guatemala, *J.*  
 1178 *Volcanol. Geotherm. Res.*, 198(1-2), 35–44, doi:10.1016/j.jvolgeores.2010.08.007.
- 1179 Scandone, R. (1979), Effusion rate and energy balance of Paricutin eruption (1943–1952),  
 1180 Michoacan, Mexico, *J. Volcanol. Geotherm. Res.*, 6(1-2), 49–59, doi:10.1016/0377-  
 1181 0273(79)90046-5.
- 1182 Scharff, L., F. Ziemer, M. Hort, A. Gerst, and J. B. Johnson (2012), A detailed view into  
 1183 the eruption clouds of Santiaguito volcano, Guatemala, using Doppler radar, *J. Geophys.*  
 1184 *Res. Solid Earth*, 117(4), n/a–n/a, doi:10.1029/2011JB008542.
- 1185 Schilling, S. P., R. Thompson, J. Messerich, and E. Y. Iwatsubo (2008), Use of Digital  
 1186 Aerophotogrammetry to Determine Rates of Lava Dome Growth, Mount St. Helens,  
 1187 Washington, 2004–2005, in *A Volcano Rekindled Renewed Erupt. Mt. St. Helens 2004–*  
 1188 *2006, U.S. Geol. Surv. Prof. Pap. 1750*, vol. 2001, edited by D. R. Sherrod, W. E. Scott,  
 1189 and P. H. Stauffer, chap. 8, pp. 145–167, U.S. Geological Survey, Reston, VA.

- 1190 Segall, P., P. Cervelli, S. Owen, M. Lisowski, and A. Miklius (2001), Constraints on dike  
 1191 propagation from continuous GPS measurements, *J. Geophys. Res.*, *106*(B9), 19,301,  
 1192 doi:10.1029/2001JB000229.
- 1193 Segall, P. (2005), *Earthquake and volcano deformation*, 517 pp., Princeton University  
 1194 Press, doi:10.1002/0471743984.vse7429.
- 1195 Segall, P. (2013), Volcano deformation and eruption forecasting, *Geol. Soc. London, Spec.*  
 1196 *Publ.*, *380*(1), 85–106, doi:10.1144/SP380.4.
- 1197 Sheldrake, T. E., R. S. J. Sparks, K. V. Cashman, G. Wadge, and W. P. Aspinall (2016),  
 1198 Similarities and differences in the historical records of lava dome-building volcanoes:  
 1199 Implications for understanding magmatic processes and eruption forecasting, *Earth Sci.*  
 1200 *Rev.*, *160*, 240–263, doi:10.1016/j.earscirev.2016.07.013.
- 1201 Simkin, T., L. Siebert, L. McClelland, D. Bridge, C. Newhall, and J. H. Latter (1981),  
 1202 *Volcanoes of the world: A regional directory, gazetteer, and chronology of volcanism dur-*  
 1203 *ing the last 10,000 years*, viii, 232 pp., Hutchinson Ross Pub. Co., New York.
- 1204 Siswamidjyo, S., I. Suryo, and I. Yokoyama (1995), Magma eruption rates of Merapi  
 1205 volcano, Central Java, Indonesia during one century (1890–1992), *Bull. Volcanol.*, *57*(2),  
 1206 111–116, doi:10.1007/BF00301401.
- 1207 Sparks, R. S. J. (1997), Causes and consequences of pressurisation in lava dome eruptions,  
 1208 *Earth Planet. Sci. Lett.*, *150*(3–4), 177–189, doi:10.1016/S0012-821X(97)00109-X.
- 1209 Sparks, R. S. J., and W. P. Aspinall (2004), Volcanic activity: frontiers and challenges in  
 1210 forecasting, prediction and risk assessment, *State Planet Front. Challenges Geophys.*  
 1211 *Geophys. Monogr. Ser.*, *150*, 359–373, doi:10.1029/150GM28.
- 1212 Sparks, R. S. J., S. R. Young, J. Barclay, E. S. Calder, P. Cole, B. Darroux, M. A. Davies,  
 1213 T. H. Druitt, C. Harford, R. Herd, M. James, A. M. Lejeune, S. Loughlin, G. Nor-  
 1214 ton, G. Skerit, M. V. Stasiuk, N. S. Stevens, J. Toothill, G. Wadge, and R. Watts  
 1215 (1998), Magma production and growth of the lava dome of the Soufrière Hills Vol-  
 1216 cano, Montserrat, West Indies: November 1995 to December 1997, *Geophys. Res. Lett.*,  
 1217 *25*(18), 3421–3424, doi:10.1029/98GL00639.
- 1218 Swanson, D. A., and R. T. Holcomb (1990), Regularities in Growth of the Mount St. He-  
 1219 lens Dacite Dome, 1980–1986, in *Lava Flows Domes*, vol. 2, pp. 3–24, Springer  
 1220 Berlin Heidelberg, doi:10.1007/978-3-642-74379-5.
- 1221 Thouret, J.-C. (1999), Volcanic geomorphology—an overview, *Earth-Science Rev.*, *47*(1),  
 1222 95–131, doi:10.1016/S0012-8252(99)00014-8.

- 1223 Vallejo Vargas, S., K. Kelfoun, A. Diefenback, P. Ramon, F. Vasconez, M. F. Naranjo,  
1224 and G. Pino (2015), Numerical simulations of lava flows. A calibration from  
1225 thermal images of lava emplacement at El Reventador volcano, poster presented  
1226 at *26th Int. Union Geol. Geophys. Gen. Assem.*, Prague, 22 June–2 July 2015.  
1227 [http://www.researchgate.net/publication/294729286\\_Vallejo\\_et\\_al\\_IUGG-2015](http://www.researchgate.net/publication/294729286_Vallejo_et_al_IUGG-2015)
- 1228 Van Manen, S. M., J. Dehn, and S. Blake (2010), Satellite thermal observations of the  
1229 Bezymianny lava dome 1993-2008: Precursory activity, large explosions, and dome  
1230 growth, *J. Geophys. Res. Solid Earth*, *115*(8), B08,205, doi:10.1029/2009JB006966.
- 1231 Voight, B., R. P. Hoblitt, A. B. Clarke, A. B. Lockhart, A. D. Miller, L. Lynch, and  
1232 J. McMahon (1998), Remarkable cyclic ground deformation monitored in real-time on  
1233 Montserrat, and its use in eruption forecasting, *Geophys. Res. Lett.*, *25*(18), 3405–3408,  
1234 doi:10.1029/98GL01160.
- 1235 Wadge, G. (1981), The variation of magma discharge during basaltic eruptions, *J. Vol-*  
1236 *canol. Geotherm. Res.*, *11*(2-4), 139–168, doi:10.1016/0377-0273(81)90020-2.
- 1237 Wadge, G. (1982), Steady state volcanism: evidence from eruption histories of  
1238 polygenetic volcanoes, *J. Geophys. Res.*, v. 87(no. B5), p. 4035–4049, doi:  
1239 10.1029/JB087iB05p04035.
- 1240 Wadge, G. (1983), The magma budget of Volcan Arenal, Costa Rica from 1968 to 1980,  
1241 *J. Volcanol. Geotherm. Res.*, *19*(3-4), 281–302, doi:10.1016/0377-0273(83)90115-4.
- 1242 Wadge, G., B. Scheuchl, and N. F. Stevens (2002), Spaceborne radar measurements of the  
1243 eruption of Soufrière Hills Volcano, Montserrat, *Geol. Soc. London, Mem.*, *21*(1), 583–  
1244 594, doi:10.1144/GSL.MEM.2002.021.01.27.
- 1245 Wadge, G., D. Oramas Dorta, and P. Cole (2006a), The magma budget of Volcán Are-  
1246 nal, Costa Rica from 1980 to 2004, *J. Volcanol. Geotherm. Res.*, *157*(1-3), 60–74, doi:  
1247 10.1016/j.jvolgeores.2006.03.037.
- 1248 Wadge, G., G. Mattioli, and R. Herd (2006b), Ground deformation at Soufrière Hills Vol-  
1249 cano, Montserrat during 1998–2000 measured by radar interferometry and GPS, *J. Vol-*  
1250 *canol. Geotherm. Res.*, *152*(1-2), 157–173, doi:10.1016/j.jvolgeores.2005.11.007.
- 1251 Wadge, G., R. Herd, G. Ryan, E. S. Calder, and J.-C. Komorowski (2010), Lava produc-  
1252 tion at Soufrière Hills Volcano, Montserrat: 1995–2009, *Geophys. Res. Lett.*, *37*(19),  
1253 n/a–n/a, doi:10.1029/2009GL041466.
- 1254 Wadge, G., P. Cole, A. Stinton, J.-C. Komorowski, R. Stewart, A. Toombs, and Y. Leg-  
1255 endre (2011), Rapid topographic change measured by high-resolution satellite radar at

- 1256       Sourfrière Hills Volcano, Montserrat, 2008–2010, *J. Volcanol. Geotherm. Res.*, *199*(1-2),  
1257       142–152, doi:10.1016/j.jvolgeores.2010.10.011.
- 1258       Wadge, G., B. Voight, R. S. J. Sparks, P. D. Cole, S. C. Loughlin, and R. E. A. Robertson  
1259       (2014b), Chapter 1 An overview of the eruption of Soufriere Hills Volcano, Montserrat  
1260       from 2000 to 2010, *Geol. Soc. London, Mem.*, *39*(1), 1–40, doi:10.1144/M39.1.
- 1261       Wadge, G., D. G. Macfarlane, H. M. Odbert, A. Stinton, D. A. Robertson, M. R. James,  
1262       and H. Pinkerton (2014a), Chapter 13 AVTIS observations of lava dome growth at  
1263       Soufriere Hills Volcano, Montserrat: 2004 to 2011, *Geol. Soc. London, Mem.*, *39*(1),  
1264       229–240, doi:10.1144/M39.13.
- 1265       Walker, G. P. L., A. T. Huntingdon, A. T. Sanders, and J. L. Dinsdale (1973), Lengths of  
1266       Lava Flows [and Discussion], *Philos. Trans. R. Soc. A Math. Phys. Eng. Sci.*, *274*(1238),  
1267       107–118, doi:10.1098/rsta.1973.0030.
- 1268       Walter, T. R., D. Legrand, H. D. Granados, G. Reyes, and R. Arámbula (2013), Volcanic  
1269       eruption monitoring by thermal image correlation: Pixel offsets show episodic dome  
1270       growth of the Colima volcano, *J. Geophys. Res. Solid Earth*, *118*(4), 1408–1419, doi:  
1271       10.1002/jgrb.50066.
- 1272       Watts, R. B., R. A. Herd, R. S. J. Sparks, and S. R. Young (2002), Growth patterns and  
1273       emplacement of the andesitic lava dome at Soufrière Hills Volcano, Montserrat, *Geol.*  
1274       *Soc. London, Mem.*, *21*(1), 115–152, doi:10.1144/GSL.MEM.2002.021.01.06.
- 1275       Werner, C., U. Wegmüller, T. Strozzi, and A. Wiesmann (2000), Gamma  
1276       SAR and interferometric processing software, *Proc. ERS-Envisat Symp.*,  
1277       <http://citeseerx.ist.psu.edu/viewdoc/summary?doi=10.1.1.20.6363>.
- 1278       Werner, C., U. Wegmüller, T. Strozzi, and A. Wiesmann (2002), Processing strategies for  
1279       phase unwrapping for INSAR applications, *Proc. of EUSAR 2002 - 4th European Confer-*  
1280       *ence on Synthetic Aperture Radar*, *1*, 353–356.
- 1281       Woods, A. W., and T. Koyaguchi (1994), Transitions between explosive and effusive erup-  
1282       tions of silicic magmas, *Nature*, *370*(6491), 641–644, doi:10.1038/370641a0.
- 1283       Woods, A. W., and H. E. Huppert (2003), On magma chamber evolution during slow effu-  
1284       sive eruptions, *J. Geophys. Res.*, *108*(B8), 2403, doi:10.1029/2002JB002019.
- 1285       Wright, R. (2016), MODVOLC: 14 years of autonomous observations of effusive volcan-  
1286       ism from space, *Geol. Soc. London, Spec. Publ.*, *426*(1), 23–53, doi:10.1144/SP426.12.
- 1287       Xu, W., and S. Jónsson (2014), The 2007–8 volcanic eruption on Jebel at Tair island (Red  
1288       Sea) observed by satellite radar and optical images, *Bull. Volcanol.*, *76*(2), 795, doi:

1289 10.1007/s00445-014-0795-9.

1290 Yang, X.-M., P. M. Davis, and J. H. Dieterich (1988), Deformation from inflation of a  
1291 dipping finite prolate spheroid in an elastic half-space as a model for volcanic stressing,  
1292 *J. Geophys. Res.*, 93(B5), 4249, doi:10.1029/JB093iB05p04249.

1293 Zharinov, N. A., and Y. V. Demyanchuk (2008), The growth of an extrusive dome on  
1294 Shiveluch Volcano, Kamchatka in 1980–2007: Geodetic observations and video sur-  
1295 veys, *J. Volcanol. Seismol.*, 2(4), 217–227, doi:10.1134/S0742046308040015.